Photon Flux Monitor for the BGO-OD experiment

Thomas Zimmermann

Diplomarbeit in Physik
angefertigt im Physikalischen Institut

vorgelegt der
Mathematisch-Naturwissenschaftlichen Fakultät
der
Rheinischen Friedrich-Wilhelms-Universität
Bonn

Januar 2012

Ich versichere, dass ich diese Arbeit selbstständig verfasst und keine anderen als die angegebenen Quellen und Hilfsmittel benutzt sowie die Zitate kenntlich gemacht habe.

Referent: Prof. Dr. Hartmut Schmieden
Koreferent: PD Dr. Jörg Pretz

"The reason I call myself by my childhood name is to remind myself that a scientist must also be absolutely like a child. If he sees a thing, he must say that he sees it, whether it was what he thought he was going to see or not. See first, think later, then test. But always see first. Otherwise you will only see what you were expecting. Most scientists forget that. So the other reason why I call myself Wonko the Sane is so that people will think that I am a fool. That allows me to say what I see when I see it. You can't possibly be a scientist if you mind people thinking that you're a fool."

Wonko the Sane, from So Long, and Thanks for All the Fish by Douglas Adams

Contents

Chapter 1

Introduction

In 1911 Ernest Rutherford published the results of his studies of scattering alpha particles at a gold foil. Until then it was believed that the atom consists of a homogenous mass with a positive charge filling the whole space of the atom and the negatively charged electrons are placed in there, like it was described by the atom model of J.J. Thomson According to the atom model of Thomson, the probability that a alpha particle gets scattered by the gold foil must be very high. But Rutherford discovered that most of the alpha particles pass the gold foil unscattered and concluded from this discovery that most of the space of the atom must be empty. To describe this behavior the cross section was introduced, where the probability of hitting a particle is given by the ratio of the cross section to the total targeted area. This discovery was the first step to the current atom model, where nearly the whole mass of the atom is concentrated in the nucleus in the center of the atom. In 1913 Niels Bohr modified the atom model of Rutherford based on quantum mechanics. He predicted a positively charged core that is surrounded by negatively charged electrons on circular orbits around the nucleus. But according to this model every atom should emit radiation, because the atom contains accelerated charged particles. Therefore in 1928 the orbital model was developed by solving the Schrödinger equation for the hydrogen atom, where the electrons are described as standing waves. This model was the first that could properly describe the excitation spectrum of a atom.

But already in 1919 it was discovered that even the atomic nucleus of heavier atoms does not consist of a single solid particle, but several hydrogen cores. Whereas the hydrogen core was named proton. In the year 1932 Sir James Chadwick discovered a neutral particle with a similar mass then the proton: the neutron, which was identified as another particle of the atomic nucleus. Also these particles can get excited, but until know it is not possible to describe there spectra correctly. Due to quantum mechanics and the discoveries of several high energy particle accelerators we know that the nucleons consist of three quarks with two different quark flavors (up and down). Today also four other quark flavors are known: strange, charm, bottom and top. Every quark has either a electric charge of $+\frac{2}{3}e$ or $-\frac{1}{3}e$ and one of the three color charges, which belong to the strong force. In contrary to the electromagnetic force, which coupling strength decreases with the distance between the particles, the coupling strength of the strong force (α_S) increases. For small distances with $\alpha_S << 1$ the interaction due to the strong force is well described by perturbative QCD. But for larger distances, in the order of the size of the nucleons, the quarks are confined and cannot be described by perturabtive QCD. Therefore different models were developed to describe the excitation spectra observed during several experiments. But all these models are predicting much more excited states then observed during the experiments, so that these excited states and therefore the nucleons have to be investigated further.

Therefore the BGO-OD experiment, which is described in chapter 2, is set up to investigate the meson photo-production at the nucleon. Among other properties the experiment wants to measure absolute cross sections for the different reactions. To measure the cross section it is essential to know the photon flux through the experiment. For this purpose a photon flux monitor was build and installed in the experiment, which is described in this thesis.

Chapter 2

BGO-OD Experiment at ELSA

The BGO-OD experiment is located at the electron accelerator ELSA and is founded by the DFG[1], within the trans regional collaborative research center 16 “Subnuclear Structure of Matter”. The goal of the experiment is the further investigation of the inner structure of strongly interacting particles. Due to the BGO ball and the magnetic forward spectrometer with the large open dipole magnet, which are giving the name to the experiment (**BGO-O**pen**D**ipole), the experiment is especially suited for reactions with charged and neutral particles in the final state.

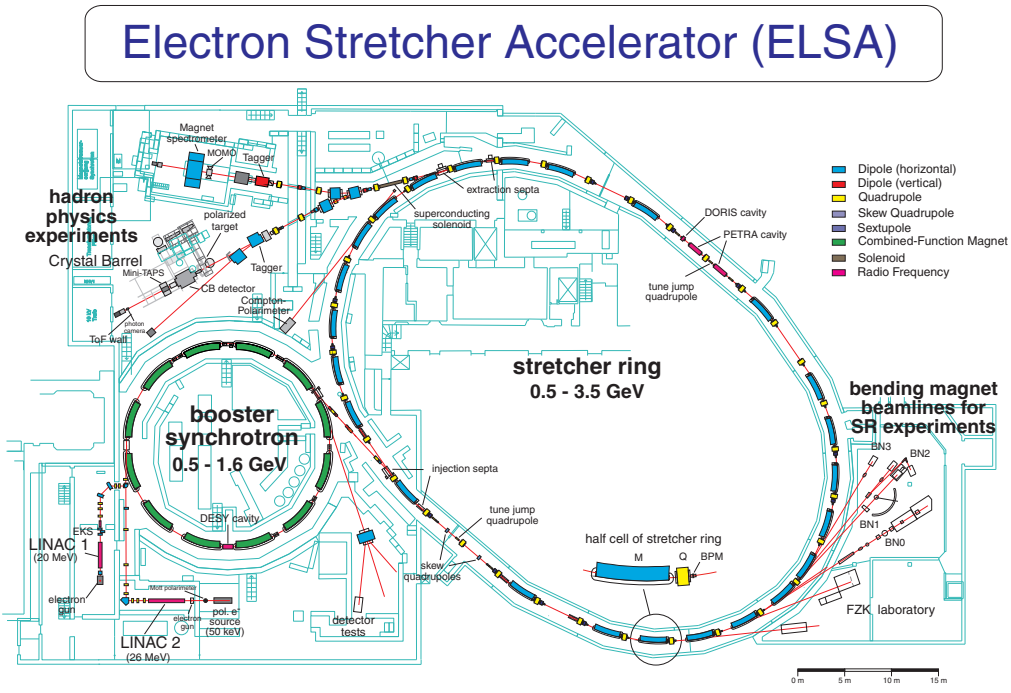

Figure 2.1: Overview of the ELSA accelerator

[1] Deutsche Forschungs Gesellschaft

2.1 ELSA

The **EL**ektronen-**S**tretcher-**A**nlage ELSA is a electron accelerator located at the physical institute of the university of Bonn, and is operated by the country of North Rhine-Westphalia. It consists of three parts, the injection LINAC, the booster synchrotron and the stretcher ring. Due to different electron sources the accelerator can provide an unpolarized and also a polarized beam of electrons with variable energy of up to 3.5 GeV [ELS05]. For the hadron experiments a current of several nA can be extracted to the two experimental areas.

The two experiments located in the two extraction areas are the Crystal Barrel Experiment[CB] and the BGO-OD experiment.

2.2 BGO-OD Experiment

The BGO-OD experiment is a fixed target experiment and consist of the BGO ball, which was formerly used at the GRAAL experiment in Grenoble and the forward spectrometer with the large open dipole magnet. The components of the experiment are shown in figure 2.2 and explained in the following sections.

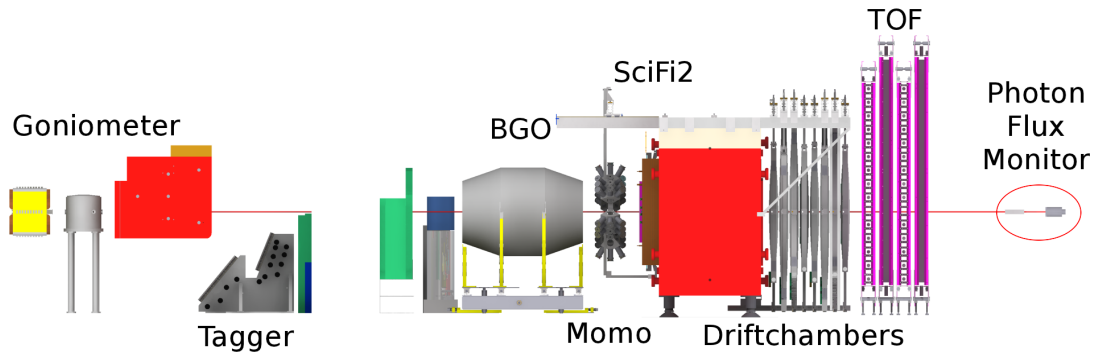

Figure 2.2: Overview of the BGO-OD experiment.

In figure 2.2 the electron beam enters from the left and generates a photon beam due to a radiator inside the goniometer by bremsstrahlung. The electrons are deflected by the tagging magnet, and those who have produced a photon are detected by the tagging detector, from which one can calculate the energy of the generated photon by the bending radius in the magnetic field of the tagging magnet. Behind the tagging detector the electron beam is dumped into the beam dump, so that the electrons don't interfere with the further experiment. The photon beam goes, inside the photon beam line, through the beam dump and hits the target inside the BGO-ball. Some of the photons do a reaction and the result of this reaction is detected by BGO-ball or, if they leave the BGO-ball in forward direction, by the forward spectrometer. The forward spectrometer consists of a large dipole magnet and several tracking detectors in front of and behind the magnet, as well as a time of flight detector.

From the tracking detectors one gets one track segment before the magnet and one behind it, so that one can calculate the bending radius of the particle track inside the magnet. Together with the

centrifugal, the Lorenz force and the knowledge of the magnetic field one can calculate the momentum of the particle.

2.2.1 BGO-Ball

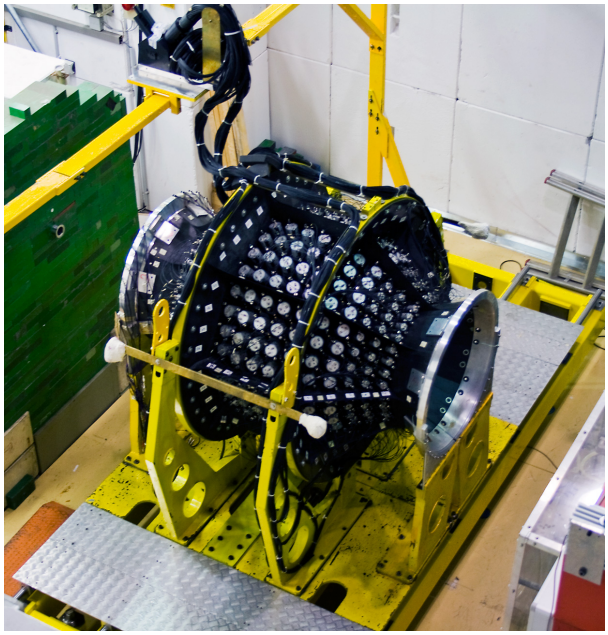

Figure 2.3: The BGO ball, without signal and HV cable.

The BGO-ball consists of 480 bismuth germanate ($Bi_4Ge_3O_{12}$, BGO) crystals, which are arranged in the shape of a lying rugby ball with a 20 cm whole in the middel. Due to this hole the photon beam line, the target and the inner detectors fit in the middle of the BGO-ball. The angle covered by the detector is 25° to 155° of the polar angle and the total azimuthal angle, so that the BGO-ball coveres nearly the whole angle around the target in the center. This makes the BGO-ball a large acceptance spectrometer for multiple photon states with excellent energy resolution.

Target

The target in the center of the BGO-ball will be hit by the photon beam and within it, the reactions will take place. The target of the BGO-OD experiment is a cryogenic cell that can either be filled with liquid hydrogen or liquid deuterium. The cell itself has a diameter of 4 cm and is available in two different lengths of 6 and 11 cm. It will be located directly inside the photon beam line, so that it is thermal isolated due to the vacuum in the beam pipe.

For easy maintenance the target system is mounted on a rail system so that it can be moved out of the beam pipe.

MWPC

Around the target pipe are a few mm left for an additional detector which will be used for tracking the reaction products inside the BGO ball. The inner detector will consist of two Multi Wire Proportional

Chamber cylinders, which are giving the name to this detector (MWPC). Each of the cylinders has two layers of strips which are twisted around a cylinder, each in another direction, and anode wires located between them. Because two strips and one anode wire cross only once, one can calculate the position of the hit from the struck channels. With two chambers on gets two points and therefore the direction the particle took inside the BGO-ball.

Silicon Strip Tracker

For tracking particles in forward direction the silicon strip detector, of the B8 subproject, will be mounted behind the target. It consists of multiple circular shaped 60 mm diameter, 300 μm thick detectors with circular or rectangular arranged silicon strips, where one hit on the front and one hit on the back can be detected. Because of the special layout of the strips, the position can be calculated from the channel numbers, where the two hits were detected. To not disturb the photon beam, the detector has a 5 mm hole in the middle.

MRPC

The particles in forward direction, with an angle of less than 25°to the beam direction, should be detected by the forward spectrometer. But the acceptance of the forward spectrometer has a maximum angle of 8°. To cover the whole forward angle an additional detector is needed, to close this acceptance hole in the experiment.

Therefore a MRPC (Multilayer Resistive Plate Chamber) will be installed between the BGO ball and the forward spectrometer. The chamber consists of several equally spaced resistive plates with a high voltage applied to the external surfaces and are filled with a special gas mixture ($96\%C_2F_4H_2$ + $3\%C_4H_{10}$ + $1\%SF_6$). Due to gas amplification the signal of an incoming particle is amplified and can be read out at the outer electrodes.

2.2.2 Forward Spectrometer

In forward direction the magnetic spectrometer with the **O**pen **D**ipole magnet is located. In front of and after the magnet, tracking detectors are installed, so that it is possible to reconstruct the track of a particle and calculate the momentum from the track radius.

Momo

The first tracking detector is MOMO; it's a scintillating fiber vertex detector with 672 fibers of 2.5 mm diameter each, which was build for the MOMO experiment at COSY. The fibers are arranged in three layers, with two modules per layer. The tree layers are rotated by 120° against each other, so that the detector covers a hexagonal area with a diameter of about 40 cm (figure 2.4). In the middle of the detector is a 5 cm hole, so that the photon beam can pass the detector. As always three of the fibers are crossing each other, the detector can achieve a spatial resolution of about 1.5 mm, and for two hits at the same time only one possible solution exists as indicated by the red, green and blue lines in figure 2.4. Two fibers are crossing at several points of the detector, but only for two points three fibers are crossing, so that the positions of these hits are unique. [MOM09]

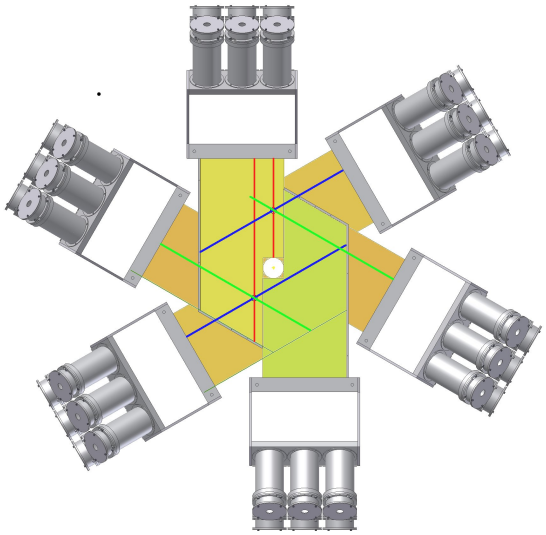

Figure 2.4: MOMO detector

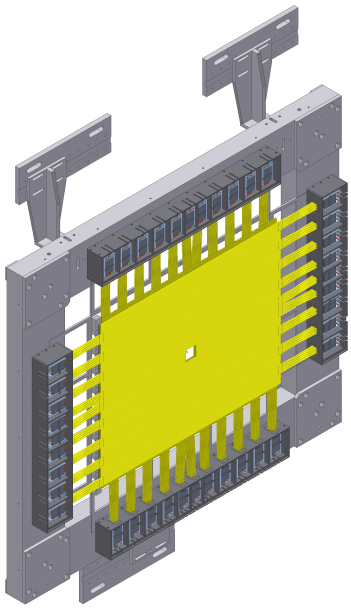

Figure 2.5: SciFi detector

SciFi2

The SciFi2 is a scintillating fiber detector consisting out of 640 fibers in two layers, which are rotated by 90° against each other and cover an area of 66 cm × 51 cm. The fibers of each layer are overlapping each other, so that every particle has to pass at least one of the fibers in each layer. The spatial resolution of this detector is about 2 mm in each direction. Also the middle of this detector a hole of 4 cm × 4 cm is spared, so that the photon beam can pass the detector without interference. [Bös11]

Open Dipole Magnet

The open dipole magnet is the central component of the forward spectrometer, as it bends the particle track and therefore enables the determination of the momentum of the particle. It is 2.8 m high, 3.9 m broad and 1.5 m deep and has a gap of 84 cm, which corresponds to an acceptance of particle trajectories of 8° in vertical and 12.1° in horizontal direction.

To reconstruct the particle tracks, and determine the momentum from these, the magnetic field of the magnet has to be known very precisely. For this purpose the magnetic field was measured at GSI in Darmstadt, as well as simulated with a very high precision.

Driftchambers

Behind the spectrometer magnet eight driftchambers are installed, two in x and two in y direction and two tilted by +9° from the vertical direction, as well as two tilted by -9°. One driftchamber consists of two layers of 77 (horizontal chamber), 144 (vertical chamber) or 152 (tilted chamber) hexagonal driftcells each and is filled with a mixture of Ar and CO_2. A driftcell consists of one signal wire, which is surrounded by six potential wires. The distance between the signal wires of the two layers is 15 mm, and the distance between two neighboring signal wires in one layer is 17 mm. Due to this geometry a spatial resolution of about 300 μm can be achieved.

The operating principle behind these chambers is, that between the signal and the potential wires an electric field is applied. The particle passing through the chamber will ionize the gas and the generated ions will then drift to one of the wires and the electron to the other one. In front of the wire gas amplification will occur, which causes a measurable signal in the wire. Because the time, the electrons need to drift through the gas is connected to the distance from the wire, one can calculate the position of the hit when one knows the time when the particle went trough the chamber. In the BGO-OD experiment this time can be get from the TOF walls or the tagger detector.

The area covered by the driftchambers is 2.5 m×1.2 m and they have an insensitive spot of 5 cm×5 cm in the middle, so that photon beam can pass trough the chamber without generating signals. [Sch10] [Ham08]

Time Of Flight Walls

The time-of-flight (TOF) detector consists of four independent walls. Each wall is build of 14 scintillating bars, 5 cm thick and 20 cm broad, with one photomultiplier at each end of the bar. Two walls have horizontal and two vertical bars, so that one can achieve a location sensitivity of 20 cm × 20 cm. The possible time resolution of the walls is $\Delta t_{1\sigma} = 0.24$ ns. [Ram07] The central bar of each wall is replaced by two aluminum dummy bars, so that also this detector provides a hole with a size of 20 cm × 20 cm for the passage of the photon beam.

2.2.3 Photon Tagging System

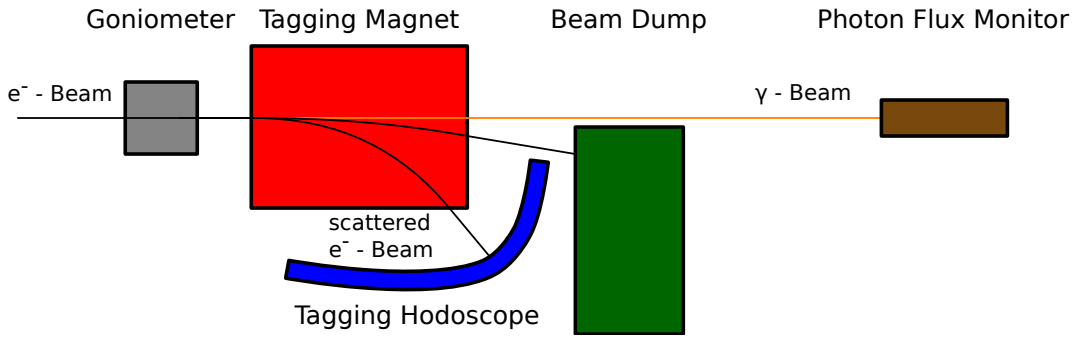

Figure 2.6: The tagging system of the BGO-OD experiment

The photon tagging systems is located in front of the experiment and it's purpose is to generate the photons needed for the experiment, as well as determine the exact energy and generation time of every single photon. The generation of the photons from the electrons delivered by ELSA, is done by bremsstrahlung with a bremsstrahl radiator in the goniometer. Determining the energy and time for these photons is done by the tagger. At the end of the experiment, the photon flux monitor will determine how many of the generated and tagged electrons really went through the experiment. As in the photon beam line, between the tagger and the actual experiment, a collimator is placed to collimate the photon beam, not all of the generated photons will arrive at the experiment.

Goniometer

The goniometer provides different bremsstrahl targets to generate the photons, from the electrons provided by ELSA, through the bremsstrahl-process. The goniometer itself consists of a radiator disk, which holds the different bremsstrahl targets, and five stages, that can move the goniometer in all three dimensions, as well as rotate the radiator disk around it's center and tilting it forth and back. Beside different sizes of copper radiators and a capton foil, which are used to generate unpolarized photons, there will also be a diamond. With this diamond linear polarized photons can be generated by coherent bremsstrahlung.

Besides the different bremstrahl targets the goniometer also holds some tools for beam diagnostics, as a cromox screen, with which one can directly observe the position of the electron beam, and horizontal, as well as vertical wires for wire scans. The wires for the wire scan can be moved through the electron beam, and by the rate of generated photons one can determine the position of the beam very precisely, as the rate will be maximal when the wire is in the middle of the beam. [Bel11]

Tagger

Behind the goniometer the tagging magnet is located, that defects all electrons with radii depending on their energy. The electrons which did not take part at the bremsstrahl process are only deflected by a small angle and go above the tagger and absorbed by the beam dump. The other electrons, that have generated a bremsstrahl photon, have lost a certain amount of energy to this photon. Therefore they are deflected by a larger angle. The more energy the electron has transferred to the photon, the more it will be deflected by the magnetic field. That way it is possible to calculate the energy of the electron and therefore the energy of the generated photon by the position the electron is detected in the tagger.

To assure a good energy resolution, the tagger should be divided in many channels, where each channel covers a small energy range. A 9 channel prototype of a tagger, for the BGO-OD experiment was build by Georg Siebke during his diploma theses [Sie10] and the total tagger with 128 channel is currently under construction.

In the current experimental installation, still a tagger with 14 channels from the SAPHIR experiment is installed and used for the analysis in this work.

Photon camera

At the end of the beam line, behind the forward spectrometer a photon camera is installed. It consist of a small converter foil and a scintillator that are mounted in an angle of 45° to the beam and a camera pointing to the scintillator with an angle of 90° to the beam. Due to the converter foil the incoming photons are converted into electrons and those are then converted into visible light by the scintillator, which is then recorded by the camera. With this device it is possible to monitor the position of the photon beam with a high precision of less then a millimeter.

Photon Flux Monitor

Even behind the photon camera at end of the beam line the photon flux monitor is located. Because of the holes in all detector components, the photons which did not undergo a reaction in the target can fly unhindered through the whole experiment. That way, the photon flux monitor at the end of the beam line can determine which of the tagged photons, were not blocked by the collimator. The photons scattered in target are also not recognized by the photon flux monitor, but the number of reactions in the target, in

comparison to the number of total photons is negligible. That way it is possible to determine the photon flux through the experiment at this position. The construction of this detector is the topic of this work.

Chapter 3

Interaction of particles with matter

To detect a particle, it has to interact with the matter of the detector. In this chapter, the interactions relevant for this work, of particles with matter will be discussed. As the BGO-OD experiment researches photon induced reactions, this chapter starts with the interaction of photons with matter. Then the bremsstrahlung process is discussed, which leads to electro-magnetic showers and the Čerenkov effect.

3.1 Interaction of photons with matter

While going through matter photons loose energy with a certain probability. For different energies and materials this occurs because of different effects. In figure 3.1 the different cross sections of the major effects are plotted for light (carbon) and heavy (lead) material. For low energies the main contribution to the cross section comes from the atomic photoelectric effect (see section 3.1.1), for middle high energies the Compton scattering (see section 3.1.2) takes over, and for high energies the pair production (see section 3.1.3) process is dominant.

There are also some other effects, e.g. rayleigh scattering and photo nuclear interactions, but their contribution to the total cross section is rather low.

For the BGO-OD experiment, the energy range above 100 MeV is relevant. In this regime the pair production process delivers the main contribution to the photon cross section, the contribution from the Compton effect is also visible, but one order of magnitude lower.

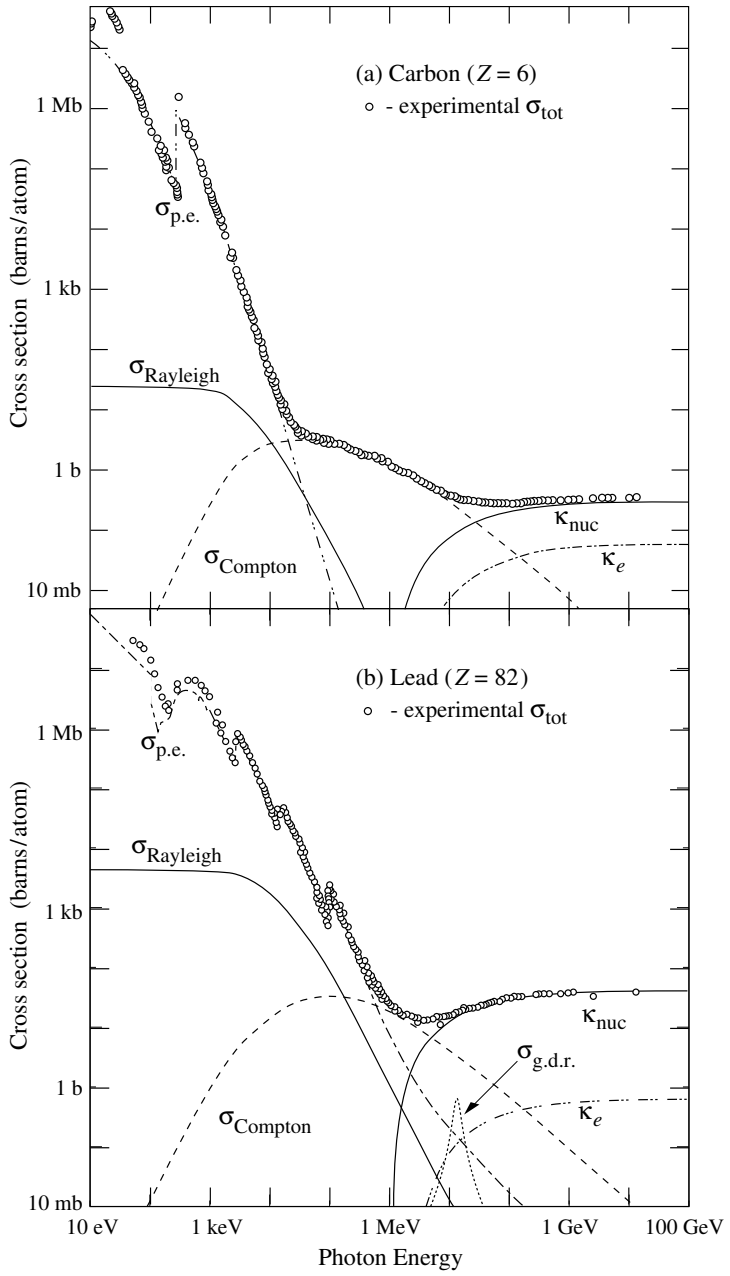

Figure 3.1: Photon total cross sections as a function of energy in carbon and lead, showing the contributions of different processes:

$\sigma_{p.e.}$ = Atomic photoelectric effect (electron ejection, photon absorption)
$\sigma_{Rayleigh}$ = Rayleigh (coherent) scattering - atom neither ionized nor excited
$\sigma_{Compton}$ = Incoherent scattering (Compton scattering off an electron)
κ_{nuc} = Pair production, nuclear field
κ_e = Pair production, electron field
$\sigma_{g.d.r.}$ = Photonuclear interactions, most notably the Giant Dipole Resonance. In these interactions, the target nucleus is broken up.

Figure taken from [NG10, Fig. 27.14]

3.1.1 Atomic Photoelectric Effect

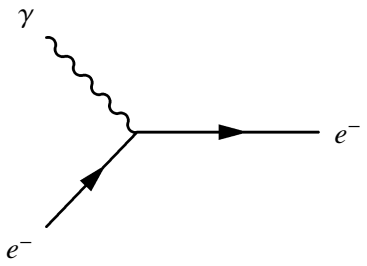

Figure 3.2: Feynman graph of the photoelectric effect

For photon energies $E_\gamma < m_e c^2$ (with the electron mass m_e and the speed of light c) the photoelectric effect is the most likely effect [Dem09, p. 93f]. The photon gets absorbed by an atom, and the energy of the absorbed photon will be transferred to the electrons. If the resulting energy of the electron energy is higher than it's binding energy, the electron will leave the atom. After this the photon is gone, and to full fill the energy and momentum conservation laws, part of the momentum has to be absorbed by the atom. Because of this, the photoelectric effect can only happen to electrons bound to an atom.

The cross section highly decreases with the electron energy. And for photon energies much lager than the binding energy of the innermost (K-level) electrons ($E_\gamma \gg E_b(K)$), the cross section is approximately given by equation 3.1.

$$\sigma \sim \frac{Z^5}{E_\gamma} \tag{3.1}$$

3.1.2 Compton Scattering

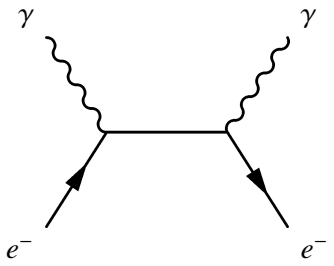

Figure 3.3: Feynman graph of compton scattering

Photons with energies of $m_e c^2 \ll E_\gamma \ll 2m_e c^2$ will most probably do (inelastic) Compton scattering. Therefor the photon is deflected at an electron and a part of the kinetic energy of the photon is transferred to the electron. Because of this the energy of the out going photon is lower than of the incoming one, and is also dependent on the scattering angle.

The differential cross section is described by the Klein-Nishina formula [Leo94]:

$$\frac{d\sigma}{d\Omega} = \frac{r_e^2}{2} \frac{1}{\left[1+\gamma\left(1+cos\Theta\right)\right]^2} \left(\frac{1+cos^2\Theta+\gamma^2\left(1-cos\Theta\right)^2}{1+\gamma\left(1-cos\Theta\right)} \right), \text{ with } \gamma = \frac{E_\gamma}{m_e c^2} \tag{3.2}$$

Where r_e the classical electron radius, E_γ the energy of the incoming photon, m_e the electron rest mass and Θ the scattering angle, under which the photon will be deflected.

Because this reaction will happen for all electrons of an atom, the cross section scales with the atomic number Z. Therefore the total cross section is depending on the photon energy and the atomic number:

$$\sigma \sim \frac{Z}{E_\gamma} \tag{3.3}$$

3.1.3 Pair Production

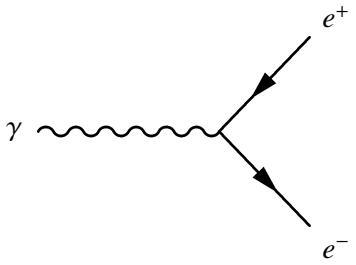

Figure 3.4: Feynman graph of pair production

For photons with even higher energy ($E_\gamma \gg 2m_e c^2$) another process dominates: the pair production. Where the energy of the photon is spontaneously converted into a electron-positron pair.

Because of the four-momentum conservation an additional particle has to be involved. This can be the atomic nuclus or one of the bound electrons of the atom. As the requirements for this process is that the incoming photon has at least the energy of the rest mass of two electrons, plus the recoil energy, there exists a minimum energy for this process:

$$E_{min} = 2m_e c^2 \left(1 + \frac{m_e}{M}\right) \tag{3.4}$$

Where m_e is the electron mass and M the mass of the particle which took over the recoil momentum. In the case of scattering at the nuclei M is much larger the m_e ($M \gg m_e$) and therefor the process starts at the energy of two electron rest masses. In the case of scattering at the electron M is equal to m_e ($M = m_e$) and therefor this process starts at energies of four electron rest masses.

For energies of $2.5\,\text{MeV} < E_\gamma < 25\,\text{MeV}$ the cross section is approximately given by:

$$\sigma \sim Z^2 \ln\left(\frac{E_\gamma}{m_e c^2}\right) \tag{3.5}$$

For higher energies the cross section increases only slowly and for energies of $E_\gamma > 500\,\text{MeV}$ the cross section is nearly constant:

$$\sigma \sim 12\alpha Z^2 r_e^2 \tag{3.6}$$

Where α is the fine structure constant and r_e the classical electron radius.

3.2 Bremsstrahlung

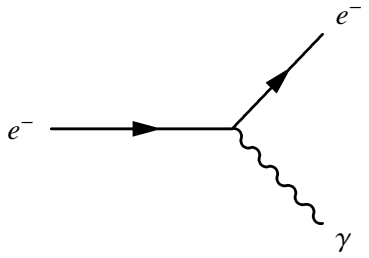

Figure 3.5: Feynman graph of bremsstrahlung

As photons aren't the only particles interacting with matter, there is also one other mechanisms that is relevant for this detector: bremsstrahlung. High energy electrons and positrons, for example produced by Compton scattering or pair production, will interact with the coulomb field of the nucleus or bound electrons.

The incoming electron enters the coulomb field of the nucleus and will be slowed down due to the electric field. The energy the electron looses will be converted into a photon. The probability for an electron with energy E_{e^-} to generate a bremsstrahl photon in the energy interval $[k, k+dk]$ while passing a layer with the thickness dx is given by:

$$P(E_{e^-}, k)dx\,dk = F(E_{e^-}, k)\frac{dx}{X_0}\frac{dk}{k} \tag{3.7}$$

Because $F(E_{e^-}, k)$ can be approximated in first order by 1, and X_0 is a material constant, the probability to emit a photon with energy k behaves approximately like $\frac{1}{k}$ [Loh90].

A concurrent process to the bremsstrahlungs process is the process of ionization losses, where the incoming electron looses energy through ionizing atoms in the bremsstrahl target. The ionization loss is proportional to the logarithm of the electron energy, and the energy when both values are equal is called critical energy E_c.

3.3 Radiation Length

High energy electrons mainly loose energy, in matter, by bremsstrahlung and high energy photons loose their energy, in matter, mostly by pair production. A length scale for this energy loss is the material dependent radiation length X_0 and it is usually measured in $\mathrm{g} \cdot \mathrm{cm}^{-2}$. It is defined by the mean distance over which the electrons looses all but $\frac{1}{e}$ of its energy, and also by $\frac{7}{9}$ or the mean free path of the photon.

X_0 is approximately given by equation 3.8 [EHO+04, Equation 27.20], where Z is the atomic number of the element.

$$X_0 = \frac{716.4\,\mathrm{g\,cm^{-2}A}}{Z(Z+1)\ln(278/\sqrt{Z})} \tag{3.8}$$

The radiation length is useful as a length scale for detectors, as one can calculate the amount of energy that will be deposited in a detector with a certain thickness.

3.4 Electromagnetic Shower and Moliere Radius

Photons generated by bremsstrahlung can be energetic enough to do pair production. The resulting electron, positron pair will again generate photons by bremsstrahlung, which can do pair production again, so that one incoming photon generates a cascade of particles. This chain will continue until the energy of all electrons is below the critical energy E_c, and these will loose there energy mainly by ionization losses.

This cascade of particles is called electromagnetic or electron-photon shower, and the number of electrons in this shower is approximately given by the energy of the incoming particle E_γ divided by the critical energy E_c:

$$N_{max} \approx \frac{E_\gamma}{E_c} \tag{3.9}$$

In a simple model, one assumes that the number of particles doubles after one radiation length. So that one has at the end of the shower, after n radiation lengths, 2^n electrons with energy E_c. From that assumption one can calculate the required longitudinal size of the detector, in radiation lengths, so that it will contain the complete shower:

$$E_\gamma = 2^n E_c \Rightarrow n \ln 2 = \ln \frac{E_\gamma}{E_c} \tag{3.10}$$

So that the maximum length of the shower (t_{max}) in radiation lengths is:

$$t_{max} \approx \ln \frac{E_\gamma}{E_c} \tag{3.11}$$

The transverse expansion of the shower is mostly given by Moliere scattering, so that this scales quite well with the Moliere radius R_M.

$$R_M = X_0 \frac{E_s}{E_c} \tag{3.12}$$

Where E_s is approximately 21 MeV and E_c the critical energy mentiond in section 3.2.

3.5 Čerenkov-Effect

Charged particles traveling through a medium, with a velocity greater than the speed of light in this medium, emit radiation with a continuos spectrum in the regime of blue light. The blueish-white light which is caused by some radioactive sources was already discovered by Pierre and Marie Curie [Cur66, p. 135], but nobody has analyzed this phenomena further; everybody believed that it's caused by luminescence. But Čerenkov discovered that this radiation can't be caused by luminescence for several reasons; like insensitivity to quenching agents, anomalous polarization or marked spacial asymmetry [icv37]. For luminescence one would expect that the addition of a quencher (e.g. silver iodide) or increase of the temperature would result in a decrease of the luminescence, because the probability that the excited atom collides with another one increases and so the energy is transferred without the emission

of light. Also light generated by luminescence should be non-polarized and isotropic, which it's not in this case; it's polarized in the direction of the incoming γ-rays and also emitted anisotropic.

The anomalous polarization and spacial asymmetry were discovered using a magnetic field. From these results, Čerenkov concluded that the source of this phenomena have to be electrons which he proved by replacing the γ-source by a β-source [Bol09].

3.5.1 Theoretical explanation

Based on these findings, Frank and Tamm [FT37] developed a theory to explain these phenomena. Frank and Tamm describe a charged particle moving through an infinite, isotropic and transparent dielectric along a straight line with constant velocity, permittivity $\varepsilon \neq 1$ and permeability $\mu = 1$, with classical Maxwell equations. The electrical field generated by this particle polarizes the medium which causes the particle to loose energy. This energy is emitted as radiation.

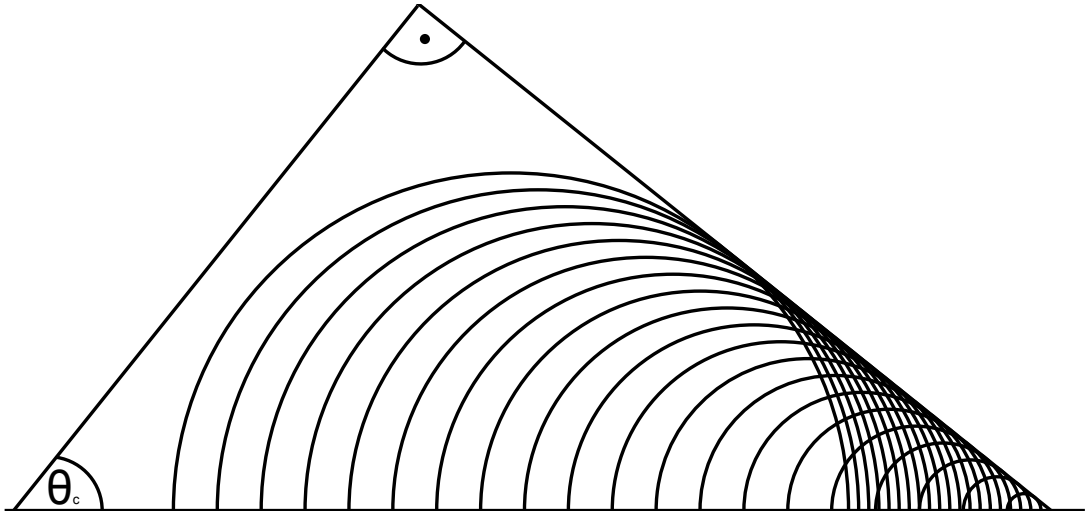

Figure 3.6: A charged particle, flowing from left to right, emitting radiation. This radiation forms a common wavefront with an angle Θ_c to the direction of motion.

Frank and Tamm found that the Maxwell equations for a system have two solutions: one for $\beta n < 1$ and one for $\beta n > 1$, where $\beta = \frac{v}{c}$ is the velocity of the particle (v) as fraction of the vacuum speed of light (c) and n the refractive index of the medium. The solution for $\beta n < 1$ results in an exponentially decreasing field, or alternatively, a not radiating particle at small velocities. For $\beta n > 1$ it describes a sum of conical waves at an angle Θ_c to the direction of motion as shown in figure 3.6. The waves from different points of the trajectory constructively interfere and build a common wavefront, like acoustical wave at the sonic boom with an opening angle Θ_c defined in equation 3.13

$$\Theta_c = \arccos \frac{1}{n\beta} \tag{3.13}$$

From the Maxwell equations not only the opening angle can be derived, but also the amount of energy, as well as the energy spectrum, can be derived. Both is described by equation 3.14 were $\frac{dW}{dl}$ is the energy loss per unit path length, Ze the charge of the particle and ω the frequency of the radiation.

$$\frac{dW}{dl} = \frac{(Ze)^2}{c^2} \int_{\beta n>1} \left(1 - \frac{1}{\beta^2 n^2}\right) \omega d\omega \tag{3.14}$$

The complete derivation can be found in [Zre70, page 1-9].

Chapter 4

Photon Flux Monitoring

One result of the experiment will be the determination of the cross section for the investigated reactions. By the determination of the photon flux through the experiment it is possible to conclude these cross sections. The particles, generated by these reactions, are detected and identified by the experiment, and from these one can conclude the reaction that has happened in the target. One can count the number of a certain reaction which has happened during a specific time, and if one also knows how many photons did not contribute to this reaction during the specific time span, one gets the probability for this specific reaction. And this probability translates directly to the absolute cross section for this specific reaction.

Therefor this chapter will explain how to determine the photon flux through the experiment. It will start with the different methods to count photons and will come to the different requirements for detector.

4.1 Concept of counting photons

For counting photons there are mainly two ways. The obvious method would be just to count every single photon. With that method one can directly see the flux from the recorded data; which is the big advantage of this type of photon counting device. But this method also requires that one doesn't overlook a single photon, and ensuring this, makes building the detector very challenging, especially when the number of photons per second is very high.

Another method would be to count only a fixed fraction of the photons. If this fraction is known and independent of the energy and rate one can calculate the real number of photons. But the first challenge with that method is to ensure that the fraction the photon counting device is counting is really independent of energy, rate and everything else. The second challenge is to know the exact value of this fraction.

Determining this fraction can be done again in different ways. The first way would be to measure an already known cross section, e.g. the π^0 cross section, and calculate the fraction from the measured values. The second way, to get this fraction, would be to use a detector, like in the first method, which counts the number of photons correctly, at least up to a certain rate. Then one can use this detector to find the fraction of photons the fixed fraction detector is counting at low rates. As the fraction is independent of the rate, the fraction calculated for these low rates will be the same as the fraction for the high rates, at which the measurements of the experiment will take place.

4.2 Requirements

As the flux monitor has to count all photons passing through the experiment, it needs to have a large enough surface, to cover the complete surface area of the photon beam. It also needs to be able to determine number of photons precisely. Depending on the method used for counting the photons it needs an efficiency of 100% for detecting photons, or at least a fix, known efficiency. The detector does

not need to count only one, but 50 million photons per second, as this is the desired photon rate the BGO-OD experiment wants to achieve.

4.2.1 Spacial Dimensions

As the beam from all these photons has a certain diameter, the detector has to be at least as large as the beam. For the Crystal-Barrel experiment [CB] in the neighboring area 99% of the beam is located within an area of $6 \times 6\text{cm}^2$ at the GIM detector [Die08]; for the beam in the BGO-OD area the expected diameter is smaller, because the collimator is located closer to the flux monitor.

As high energy photons are not detected directly by most detector types, but first converted into electrons, there are additional spacial requirements. The conversion of photons to electrons needs some additional space. In the plane perpendicular to the beam axis, the Moliere radius (section 3.3) gives an indication for the needed size. As the Moliere radius is the radius of a cylinder, that contains 99% of the shower generated by an incoming photon, one can be sure to see the photon if the detector has a diameter of two times the Moliere radius. The needed space along the beam axis is indicated by the radiation length (section 3.3). Because the photons are converted to electrons only with a certain probability at least some radiation lengths are needed, to make sure that every photon is converted and can be detected by the detector. Alternatively they have to be converted into electrons by some converter in front of the detector.

4.2.2 Rate Stability

The detector material converts the energy deposited by the particle into light, which can be detected by a photomultiplier. The signal of this photomultiplier is read out by a chain of electronic apparatus. Every part of this can effect the rate stability of the detector, either by dead time, saturation or other rate dependent effects.

Detector materials have decay times form less than 1 ns up to several μs [Der11]. When a second hit happens, before the intensity of the first signal is decreased enough to distinguish both signals, the second hit can not be seen. Because of this, the detector material needs a decay time as short as possible to be able to detect high rates.

The light from the detector material will strike the photocathode and form the absorbed energy, electrons are generated, due to the photoelectric effect. These electrons are multiplied within the photomultiplier, so that the signal from the photomultiplier has a larger amplitude, but also a broader signal than the one from the detector material. Typically the signal of a photomultiplier has a foot width of more than 10 ns, which limits the maximal constant rate, of photons, that can be detected, to $\frac{1}{10\,\text{ns}} = 100\,\text{Mhz}$. But in the experiment the rate is not constant; the arrivals of the photons are Poisson distributed, and this distribution results in exponential distributed inter arrival times, like shown in figure 4.1. This means that short distances between two photons are much more likely than large distances, but also very long distances are possible.

Additionally to the dead time of the detector material and the photomultiplier, the read out electronics adds another amount. A lot of parts work with capacitors, that need to be recharged after every signal, so that they can't process another hit, before the capacitors have reached a high enough voltage. Some other parts, mainly those with clocked logic, require a certain pulse length and break before the next signal can be processed. Signals that do not fulfill these conditions will just not be recognized.

In figure 4.1 one can see, that for 50 Mhz more than 60% [1] of the arrivals, the time between two hits

[1] $\int_{0\,\text{ns}}^{10\,\text{ns}} \mathrm{d}x\, e^{-x \cdot 50\,\text{GHz}} \cdot 50\,\text{GHz} \simeq 0.6065$

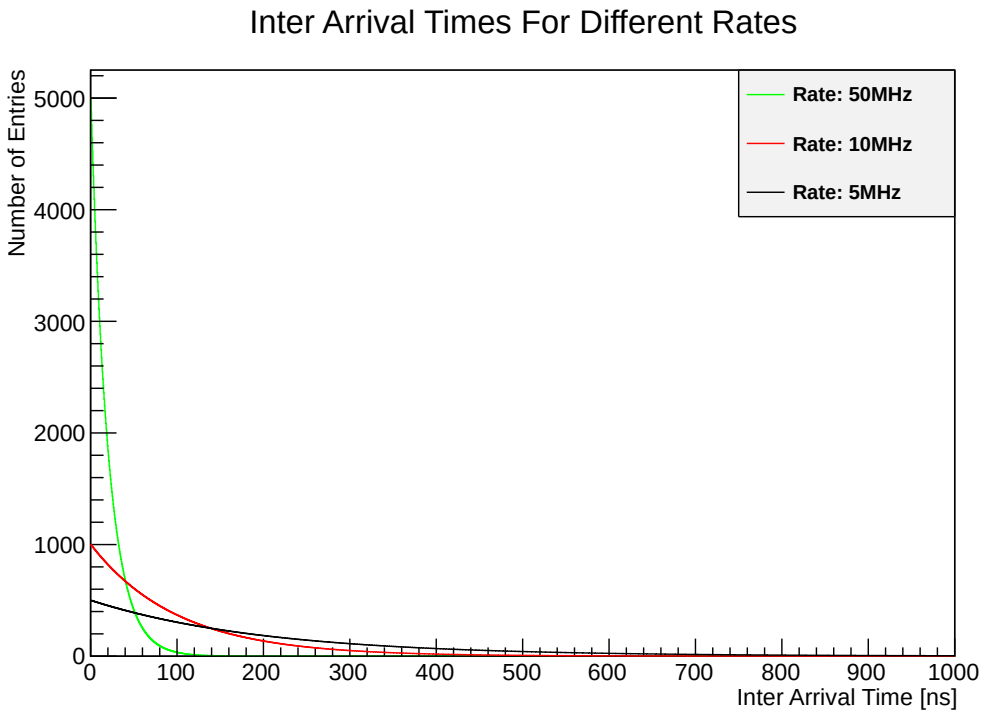

Figure 4.1: Inter arrival times of Poisson distributed arrivals for different average rates

is smaller than the pulse length of an average photomultiplier of 10 ns. This means that one won't see many of these hits.

This leads to the requirement, that the dead time, of the whole detector setup including the readout electronics, has to be as small as possible. Ideally the dead time would be zero. But because of finite pulse widths, there will always exists a certain dead time.

Chapter 5

Construction of the Photon Flux Monitor of the BGO-OD Experiment

Like mentioned in the chapter before, the photon flux monitor for the BGO-OD experiment needs to count photon rates up to 50 MHz. To full fill this requirement I've decided to split the detector into two parts: the FluMo (**Flu**x **Mo**nitor), and the GIM (**G**amma **I**ntensity **M**onitor). The GIM detector is counting all incoming photons with a precision of nearly 100%, but only for lower rates; the FluMo detector is counting a constant fraction of photons with high precision, even for high rates. To determine the fraction of photons the FluMo is counting one can compare the count rates of FluMo and GIM during a low rate period of the experiment. As the fraction of photons FluMo is counting is constant, and the GIM is counting the photons at low rate correctly, one gets the fraction just by dividing the number counted from FluMo (n_{FluMo}) by the number counted from GIM (n_{GIM}): $frac_{FluMo} = \frac{n_{FluMo}}{n_{GIM}}$.

With this fraction one can reconstruct the real number of photons (n_{real}), just by dividing the number counted from FluMo by $frac_{FluMo}$: $n_{real} = \frac{n_{FluMo}}{frac_{FluMo}}$.

The advantage of splitting the detector into two parts is, that none of both parts needs to count rates up to 50 MHz. Building a detector, that counts photon rates of 10 MHz is already very hard, as one can see from the history of the GIM detector of the Crystal Barrel experiment ([Kon01] [McG08] [Die08]). When splitting the detector it has to count only much lower rates, which are much easier to handle.

To make the determination of the fraction seen by FluMo precise, the GIM should count as high rates as possible, because this makes the error of the fraction much smaller.

In this chapter is the choice of the used components for the GIM detector described and how they were put together. After that the same is explained for the FluMo detector.

5.1 GIM - Gamma Intensity Monitor

The GIM is a total absorption detector that should have an efficiency of nearly 100% for lower photon rates. The detector consists of a big lead glass block and one photomultiplier, that is supplied with a specially made photomultiplier base that admits the photomultiplier to withstand highest rates.

5.1.1 Detector Material

To get pulses as short as possible, the detector uses the Čerenkov effect to count the photons. The pulse length of Čerenkov light is as long as the time the particle needs to travel from one end to the other, minus the time the light needs for this way. Other scintillator materials have longer pulse lengths, because additionally to that time, there is the time the scintillator scintillates.

Čerenkov light is produced by charged particles in different materials. For the A4 experiment at MAMI the most common materials were compared for there use in a Čerenkov calorimeter [Ach01,

Kapitel 2]. The result of this comparison was that PbF_2[1] is the best Čerenkov material, but lead glass is also good enough. Because there are several blocks of lead glass, in different sizes, available, I have chosen it as the Čerenkov material.

In addition to the material, also the dimensions of the lead glass block have to be large enough. All available blocks have a length of 28 cm, which translates to about 11 radiation lengths. As mentioned before, some radiation lengths would be enough, with 11 radiation lengths[2] the energy deposit in the lead glass will be more than 99.9% of the total energy of the incoming particle. With that length one can be sure to get a signal from the incoming particle, so that the available length of the lead glass blocks fits the needs for this detector. In the transverse direction, the surface of the beam needs to be covered, and because the particle makes a shower, one Moliere radius should be added around the beam. So that the detector has to cover a circle with the diameter $r = r_{Beam} + r_{Moliere}$, where in the case of the BGO-OD experiment $r_{Beam} \sim 2\,\text{cm}$ and in the case of lead glass $r_{Moliere} \sim 3\,\text{cm}$, which results in a diameter of $d = 2r \sim 10\,\text{cm}$, that needs to be covered by the detector to contain the complete electron-photon shower. The different available diameters are: 6.5 cm, 7 cm, 14 cm and 20 cm. The smaller two would have the advantage that they can be read out by a 2“ photomultiplier without light guide. The larger two have the advantage that they will contain the complete shower and a small misalignment would have no big effect on the efficiency of the detector. To absorb as much energy as possible from the shower, generated by the incoming photon, but not having to use a light guide, i have chosen the 7.5 cm block for the GIM prototype. For the final detector the larger 14 cm lead glass block was used. Through the needed light guide, to read out the detector material, the signal amplitude of the photomultiplier will be smaller, but this can be compensated by a higher amplification. The main advantage of the larger lead glass block is that it will contain the complete particle shower and therefore the whole energy of the particle, so that one can get a rough estimate of the energy of the incoming particle from the resulting pulse.

An alternative to using one big block would be using multiple small blocks: 2×2, 3×3 or 4×4. But beside the need for smaller blocks, there is no advantage because the Moliere radius is larger then the radii of these blocks and therefore the beam would always hit multiple blocks. Additionally there would be a small gap between the blocks, which would result in loosing signal amplitude or even loosing complete hits, when this gab gets stuck.

Radiation damage

Another thing one has to think about, is that an high energy particle can damage the detector material. Due to its high energy it can change the properties of the detector material. Because these changes of the properties have negative influences on the detector material, these changes are called radiation damage. For a Čerenkov detector the most important property that changes due to the high energy particles, is the transmission for visible light. This happens because the radiation generates color centers inside the crystal lattice. After a certain amount of energy deposition, the material gets yellow, brown or even black and therefore the transmission is reduced dramatically.

In figure 5.1 the transmission of different Čerenkov materials, after the absorption of 200 Gy of low energy electrons[3] are shown. 200 Gy[4] is the order of radiation exposure that one would expect for two weeks of beam time at the BGO-OD experiment. For Lead glass this will result in a decrease of the

[1] lead fluoride

[2] Radiation length of lead glass: 2.55 cm for SF-5

[3] 1.2 MeV electrons from a Cobalt 66 source

[4] $\frac{1\,\text{GeV}\cdot 10\,\text{MHz}\cdot 14\,\text{days}}{4\,\text{cm}\cdot 4\,\text{cm}\cdot 28\,\text{cm}} = 194\,\text{Gy}$

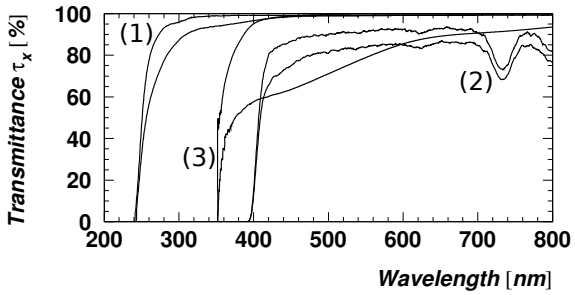

Figure 5.1: Comparison of different Čerenkov materials, before and after irradiation with 200 Gy: [Ach01, page 47]
1) Lead fluoride
2) Lucite
3) Lead glass

transmission of about 50%, so that the detector needs a maintenance period after each beam time, to heal the radian damage.

Figure 5.2: Lead glass with brown color from radiation damage.

These damages will heal on their own, and the transmission will restore itself. But this can take up to several weeks or months, until the complete detector material is 100% transparent again. But this process can be accelerated with the help of higher temperatures or the irradiation with blue or ultraviolet light. Both methods will excite the electrons inside the color center, which will then decay into the ground state of the lattice. Due to this process the color center will vanish, 100% transmission is restored and the detector can be used again.

5.1.2 Photomultiplier

To convert the photons produced in the detector material due to the Čerenkov effect into an electrical signal a photomultiplier is used. The photons hit the photo cathode on the backside of the front window, which then emits electrons due to the photoelectric effect. The electrons are then accelerated to the first intermediate electrode in the photomultiplier (dynode) due to an applied electric field. The dynode will emit a larger amount of electrons then the amount of impacting electrons by secondary emission. These electrons will then be accelerated to the next dynode, due to the next electric field, so that with every dynode the number of electrons increases exponentially. From the last dynode the electrons are then accelerated to the anode, where all electrons are collected and produce a measurable signal. The size of the signal is depending on the intensity of the incoming light, but also on the amplification of the

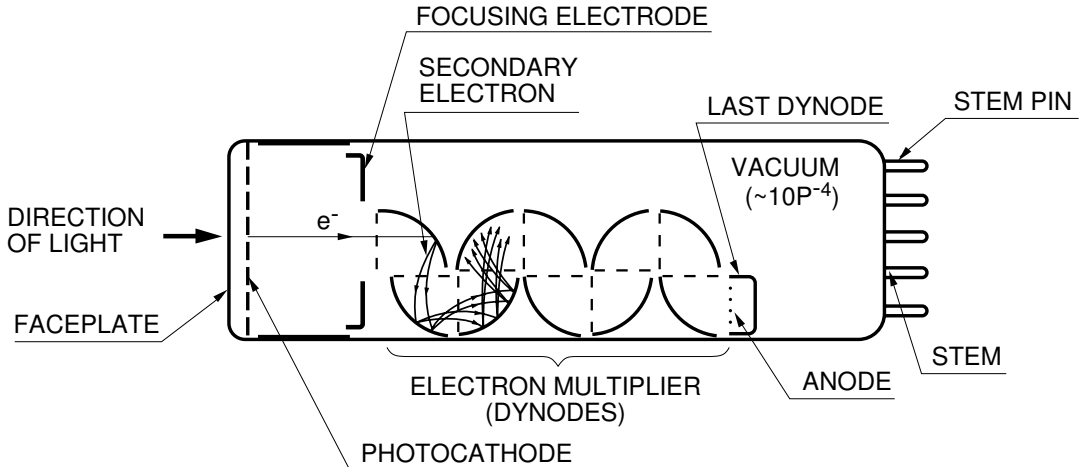

Figure 5.3: Basic schematics of a photomultiplier [Ham, page 17]

photomultiplier. This amplification is mainly affected by the number of stages and the total potential difference between cathode and anode.

Instead of using one of these photomultiplier to read out the detector material one can also use multiple photomultiplier. Each reading out one block, or multiple reading out one big block of detector material. The advantage of having multiple photomultiplier would be, that one could use smaller photomultiplier and also have the ability to triangulate the position of an incoming particle. But for the determination of the position of the beam the BGO-OD experiment has a photon camera directly in front of the photon flux monitor, which is much better suited for this job. Using smaller photomultiplier could be useful, if smaller tubes have a shorter pulse width. One could also think, that using multiple photomultiplier would reduce the rate each photomultiplier will see. But because the Moliere radius of lead glass (or $PbWO_3$ or PbF_2) is larger than the radius of a 2" photomultiplier, a hit will be seen by all photomultiplier covering the central part. Due to this all photomultiplier covering the central part will see the same (full) rate. Which means that one needs, in the case of using one photomultiplier and in the case of using multiple photomultiplier, at least one that can withstand the full photon rate.

Using one photomultiplier has the disadvantage that one needs a light guide to guide all the light into that single photomultiplier. Through this light guide a significant amount of light gets lost, but this can be compensated by a higher gain of the photomultiplier. But the big advantage is, that one can concentrate on this single photomultiplier and can spend more resources, like high voltage channel, for this single one.

The alternatives to a photomultiplier, with short pulse length, are MCP's[5] and SiPm's[6], but both are only available with very small diameters and have a much higher dead time, so that there won't be much benefit from using these, expect from shorter pulse lengths. But due to the dead time the achievable rate would be similar, or even lower.

To cover an area of the lead glass as large as possible a large photomultiplier is preferred. Also the rise time of the signals should be as short as possible. All fast and large photomultiplier I have found, are listed in table 5.1.

From this comparison one can see that the R2083 and R3377 from Hamamatsu have the shortest

[5] Micro Channel Plate
[6] Silicon Photomultiplier

Photomultiplier	**Diameter** [mm]	**Rise Time** [ns]
Hamamatsu R1584	127	2.5
Hamamatsu R1250	127	2.5
Hamamatsu R4143	76	1.8
Hamamatsu R4885	76	1.8
Hamamatsu R2083	51	0.7
Hamamatsu R3377	51	0.7
Hamamatsu R1828-01	51	1.3
Electron Tubes 9807B	51	2

Table 5.1: Comparison of different Photomultiplier larger than 50 mm

signal rise time, and all larger ones have much longer rise times. With rise times of less than 1 ns, those two are even faster than most of the smaller photomultiplier. The R2083 is also used for the TOF walls (see section 2.2.2) of the BGO-OD experiment, so that it is already available and I used one of the spares for the GIM detector.

5.1.3 Photomultiplier Bases

In contrast to the individual bars of the TOF walls, the GIM detector has to withstand a much higher rate, so that not the same standard base as for the TOF walls could be used. The purpose of the photomultiplier base is to provide the different potentials needed for the different dynodes. In the easiest case this is done by a simple voltage divider circuit, where the supply voltage is divided by resistors. Because the electrons for the multiplication, at the dynodes of the photomultiplier, are needed instantly, one adds additional capacitors in parallel. These capacitors can store a certain amount of charge and deliver it instantly to the dynode when an electron impacts. This works fine as long as there is enough time to charge the capacitor again before the next electron arrives. As an example for the schematics of such a base, the schematics of the base used for TOF is shown in figure 5.4.

Another problem occurs when the current flowing through the dynodes is in the order of the current flowing through the voltage divider. As the amplification, from one dynode to the next, is given by the voltage between those two and the voltage is given by Ohm's law, the amplification depends on the resistance and the current flowing between both dynodes. But if there is a macroscopic current flowing beside the resistor through the dynodes the total resistance is given by the parallel circuit of two resistors, which is lower than the resistance of the resistor in the voltage divider. As the current flowing between both dynodes is still the same, the voltage and therefore the amplification drops. And when the amplification drops, the size of the signal shrinks and it will be possible that the signal shrinks so much that it won't come over the detection threshold, and therefore will not be recognized be the readout electronics.

To workaround the last problem, one can replace the resistors by transistors and Zehner-diodes, like it is done for the bases of the Crystal-Barrel GIM (Figure 5.5), which is then called an active or transistor base. This type of base solves the problem that the amplification drops when the current through the dynodes gets to large. Because the resistive voltage divider is now only used as a voltage reference and the current for the dynodes is flowing through the transistors, so that the voltage divider is always loaded in the same way. If the load does not change, the resistance between two points in the voltage divider won't change and therefore the voltage won't change.

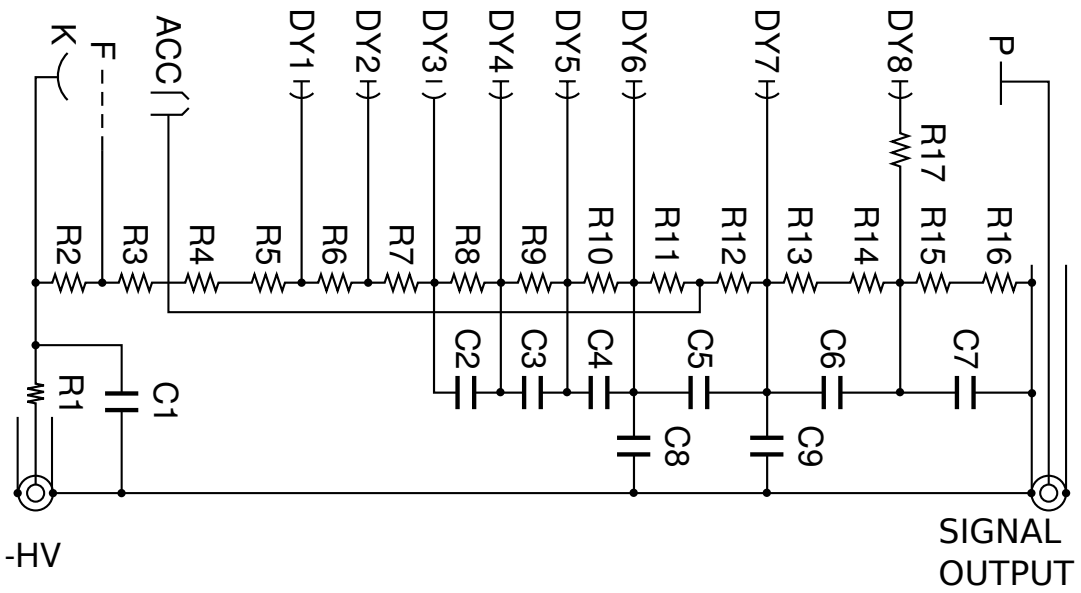

Figure 5.4: Schematics of the passive photomultiplier base used by TOF [Ham, page 79]

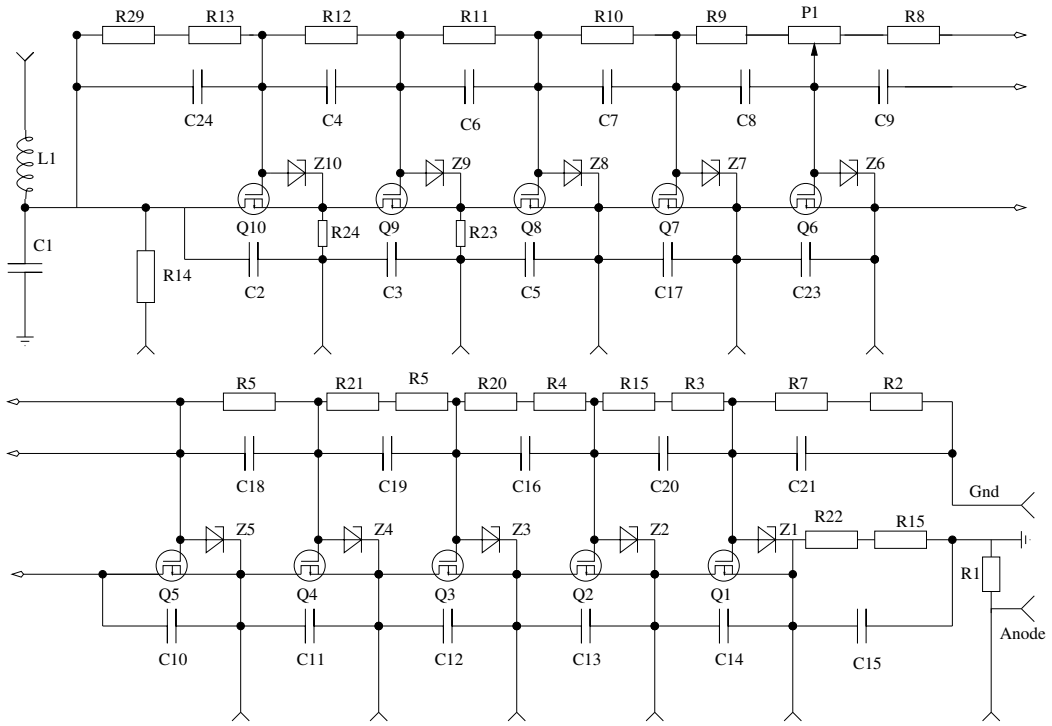

Figure 5.5: Schematics of an active photomultiplier base used by the GIM of Crystal Barrel [Kon01, page 25]

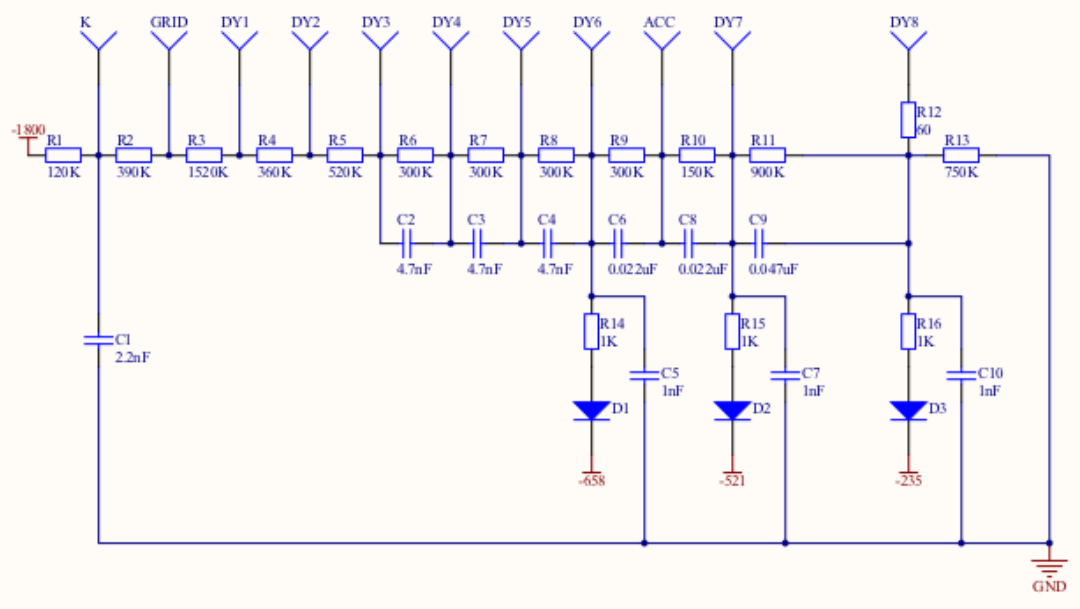

Figure 5.6: Schematics of the photomultiplier base used for the GIM detector

But still this is not the optimal case; due to limitations of the transistors it is possible that the charge is still not delivered to the dynodes in time. And when there are not enough electrons available, the amplification will drop. To solve this problem, one can add an additional high voltage power supply to the last dynodes, where this problem especially occurs. The electrons can be delivered much faster to the these dynodes, as they are directly connected to a high voltage without any components that would limit the current.

This type of base is called booster base, because the last dynodes are ”boosted“, and it is the one that assures the highest rate stability [YYO+96]. A booster base consists out of a ”normal“ passive photomultiplier base with additional high voltages connected to the last dynodes. Due to this, the current through the voltage divider is constant, as the first stages do not drain much current and the last stages get there current from the additional high voltage supply, so that with this circuit the amplification is constant.

The booster base for the GIM detector consists of a voltage divider, that has the same values as the voltage divider of TOF, and additionally three booster stages for the last three dynodes. The booster stages have a diode build in, to prevent current from flowing back into the power supply. The schematics of this base is shown in figure 5.6.

5.1.4 Prototype

The booster base for the GIM prototype detector was build by Johannes Goetze during his BCGS[7] research internship [Goe11]. The design for this base was based on the design of the TOF base, where the components are directly soldered to the socket. The advantage of this construction is that it can be done without the help of an external company, and therefore in a short time. But putting this amount of components on such a small space makes the base hard to build (figure 5.7). This base, together with with a Hamamatsu R2083 photomultiplier and a lead glass block of 7 cm × 7 cm × 28 cm are the

[7] Bonn Cologne Graduate School

main components of the first prototype of the GIM detector. As housing a square iron tube was used, which should also act as a shielding against the magnetic stray field from the open dipole magnet, that is located only three meters away. To hold the lead glass in the right position inside the iron tube, two, three-layer-paperboard stands were used (see figure 5.8). The photomultiplier was fixed to the lead glass block with tape, and for the optical contact between the photomultiplier and the lead glass, optical grease (NE 588) was used.

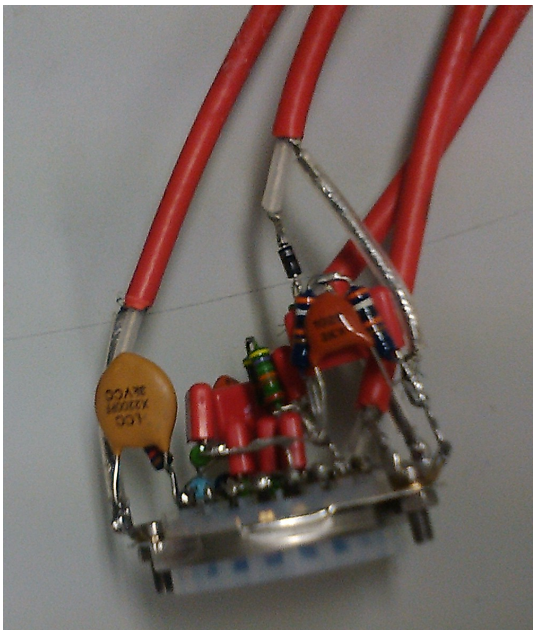

Figure 5.7: Booster base build by Johannes Goetze for the GIM detector.

Figure 5.8: GIM prototype front view, without cover. The lead glass is placed in the iron tube with a paperboard stand and through the lead glass, the photo cathode of the photomultiplier is visible.

A good optical contact without any air bubbles is important, as if the refractive indexes mismatch, which would be the case for lead glass (refractive index $\sim$ 1.7) and air (refractive index $\sim$ 1), the light won't go from the lead glass to the photomultiplier and instead will be reflected, and therefore never recognized by the photomultiplier. Therefore the optical grease has a refractive index similar to the one of the detector material and the one of the window glass of the photomultiplier.

The lead glass, with the attached photomultiplier and base, was put into the iron tube and protected against light with multiple layers of black tape. The light tightness was tested by slowly increasing the supplied high voltage, and looking for cosmic particles. When the housing wouldn't be light tight, one would see much more signals than one per square centimeter and minute.

This prototype was used in the April and June beam times 2011, and proofed that the photomultiplier with booster base was working, but the lead glass block showed much more radiation damage than expected.

5.1.5 Final Design

For the final GIM detector another lead glass block was used, in the hope that this one would stand better against the radiation damage. This lead glass block was the 14 cm diameter block, mentioned in

section 5.1.1, which is also large enough to contain the complete electron-photon shower, and therefore makes it possible to determine the energy of the incoming particle, and compare this value to the energy determined by the tagger. This lead glass block already had a housing for a 2″ photomultiplier, including a suitable light guide, so that this one could be reused for the GIM detector (figure 5.9).

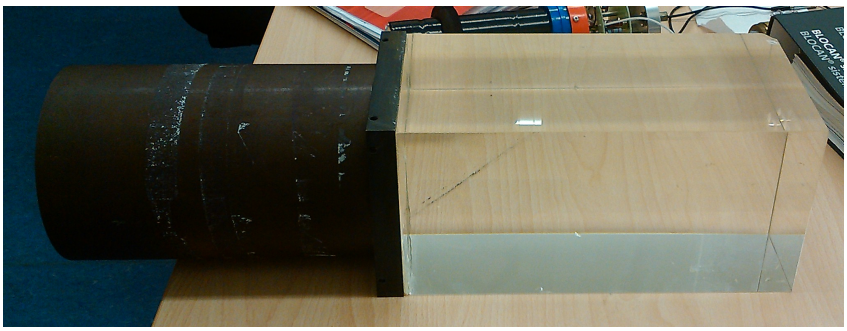

Figure 5.9: 14 cm diameter lead glass block, including the housing, which is used for the final GIM detector

The purpose of the light guide is to guide the light from the detector material to the photomultiplier. As the lead glass block is quadratic and has an edge length of 14 cm but the photomultiplier is round and has a diameter of only 5.1 cm a lot of light would be lost, if the photomultiplier would just be placed in the middle of the lead glass block. As the light should enter and leave the light guide towards the photomultiplier without being reflected the refractive index of the material has to be in the same order as the refractive indexes of the lead glass and the photomultiplier window. Also the light guide has to be transparent for the wavelength emitted by the detector material. Inside the light guide the light should not leave the light guide at the edges, but only at the side where the photomultiplier is attached. To achieve this the light guide is build in a way that the incoming light is reflected, at the walls, due to total reflection.

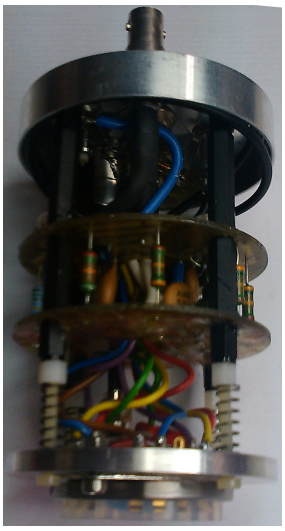

Figure 5.10: PCB based booster base for the final GIM detector.

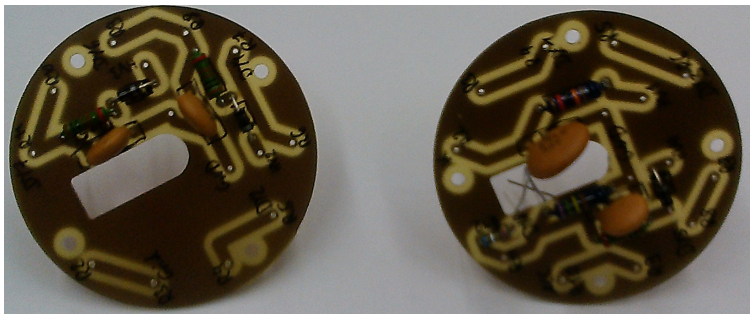

Figure 5.11: Partly equipped PCB's for the base of the final GIM detector

For the new GIM detector only the photomultiplier and the base of the old detector had to be exchanged. As the base of the prototype was a bit fragile, a new layout for the base, based on pcb's, was designed (figures 5.11 and 5.10). The most fragile parts, were the connection between the HV cables and the attached resistors or diodes. Already a small force caused this connection to break. Therefore the HV cables were connected like through hole parts to the PCB, which is a much more stable connection. Also because everything is in a fixed housing, the force on this connection does not change when touching the detector. To assure a good optical connection between the light guide and the photomultiplier a silicon cookie is used. Due to springs in the housing of the base a constant pressure is put on the silicon cookie, so that a air bubble free connection is assured.

5.2 FluMo - Flux Monitor

It is expected that the GIM detector will saturate at some rate, as the probability that two photons hit the detector within it's dead time, increases with the rate. It is expected that this will happen around a rate of 10 MHz. Therefore a solution for the high rates is needed. The chosen solution for the photon flux monitor of the BGO-OD experiment is a detector, which counts only a fraction of the photons. To have a constant fraction, independent of the photon rate, a detector based on the pair production process was build. The cross section of the pair production process is well understood and not depending on the rate of incoming photons. Also it is constant over the range of photon energies which are used in the BGO-OD experiment.

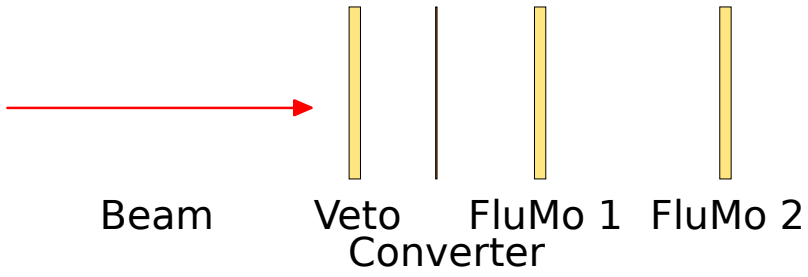

Figure 5.12: Schematic of the FluMo assembly

The pair production process will take place in a converter, which can be any type of material. The converter material mainly determines the fraction of photons, which this detector will count. This converter will be placed in front of a scintillator, which counts the produced electron-positron pairs. As the detector should only count particles produced in the converter in front of the converter a veto detector for all charged particles is installed. Also it should detect only particles produced from pair production, so that the threshold for sending a signal must be set to the energy of two minimal ionizing particles. Otherwise the electrons produced by Compton scattering would also be counted, and the cross section for this not constant over the photon energy range used in the BGO-OD experiment.

As one can see in the energy spectrum of one of the FluMo detectors (figure 5.13), the edges of the individual peaks are not easily distinguishable. To easier distinguish, the one and two electron events, a second scintillator, after the first one, is used. That way, one can easily distinguish the tail of the one electron peak from the two electron peak, because the probability, that the hit is in the tail of the one electron peak in both scintillators, is very low.

If the thresholds for both FluMo scintillators is set correctly, only events from photons converted

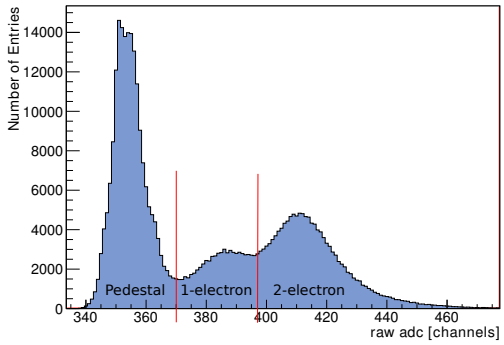

Figure 5.13: Raw ADC spectrum of one of the FluMo scintillators. The red lines mark the edges of the different peaks: pedestal, one electron peak and two electron peak.

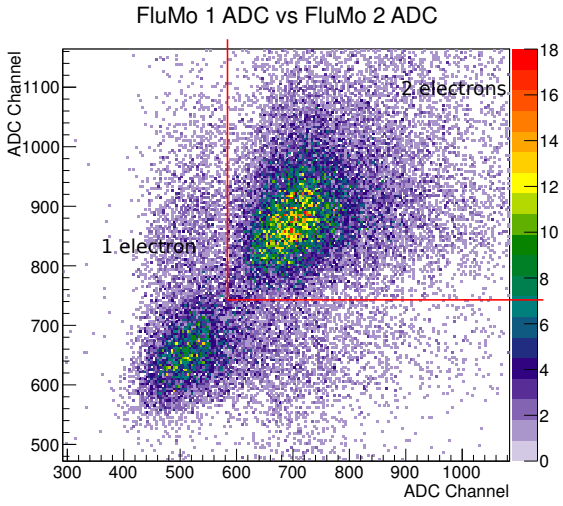

Figure 5.14: Raw ADC spectrum of one FluMo scintillator against the raw ADC spectrum of one of the other scintillator. The two peaks: one and two electron peak, are clearly visible. The pedestal is not visible, because in this histogram, only those hits are entered, where a hit in the TDC was recognized.

Channel	Threshold	Supplied high voltage
FluMo Veto	30 mV	1000 V
FluMo 1	113 mV	1050 V
FluMo 2	145 mV	1000 V

Table 5.2: Threshold for the different FluMo channel used during the beam time in December 2011

inside the converter into electron-positron pairs are recognized. The threshold is minimal amplitude of the signal from the detector. As the amplitude of the signal is larger the more energy is deposit in the detector, one can set it to a value to choose only process hits where a certain amount of energy was deposit. But the amplification of the signal is depending on the gain of the photomultiplier and therefore on the supplied HV and as well on the specific hardware, as every combination of scintillator, light guide, photomultiplier and base can be a bit different. Therefore the threshold needs to be chosen for every channel separately; in table 5.2 the settings used during the beam time in December 2011 are listed.

To determine the number of photons which arrive at the FluMo, one has to know the fraction of photons that convert to electron positron pairs. To get this, one compares the number counted by the GIM and FluMo detector at low rates, and gets the fraction just by the quotient of these two values.

5.2.1 Detector Material

The FluMo detector has to detect electrons and positrons with an high efficiency of nearly 100%, and as the rate in this detector can also be high, a short rise and decay time and a high light output are needed.

	BC-400	BC-404	BC-408
Light output [% of Anthracene]	65	68	64
Rise time [ns]	0.9	0.7	0.9
Decay time [ns]	2.4	1.8	2.1
Wavelength of max. emission [nm]	423	408	425

Table 5.3: Comparison of different plastic scintillators [Sai]

The material type, which is suited the best for this purpose, is a plastic scintillators. This scintillator is made out of a scintillating material, which means that this material emits light, when an ionizing particle deposits energy inside the material. The incoming, ionizing particle will excite electrons of the molecules of the scintillating material, which will then emit light during their de-excitation. The number of photons emitted by the scintillator is about one photon per 100 eV deposit energy [NG10, page 246]. Plastic scintillators are the most common type of scintillators, which are made of a polymer, and are very efficient when detecting charged particles, like electrons.

In table 5.3 several common and fast scintillator materials are listed, from these the BC-404 scintillator material is the fastest available. The only disadvantage of this material is it's wavelength of maximal emission, which is in the regime of ultra-violet light. As normal Plexiglas is not transparent for UV-light, one has to keep this in mind when building the light guides for these scintillators. But there exists UV transparent Plexiglas too, which can be used for the light guides.

The BC-404 scintillator has another big advantage: it will be used for the new tagger of the BGO-OD experiment, and therefore it does not need to be bought. Therefore this material was chosen for the FluMo detector.

5.2.2 Photomultiplier

The expected count rates of the FluMo detector is in the order of less than 10% of the total number of photons. As the maximal photon rate, the experiment is designed for, is 50 MHz, the FluMo photomultiplier have to withstand a rate of less than 5 MHz. This rate is similar to the rate one of the tagger bars will be exposed to.

Because the photomultiplier for the tagger are already chosen, and several spares available, these were used for the FluMo detector. The photomultiplier is a 9111SB from ET Enterprises [ET] and was delivered with a C673ASN2 base. This base is a passive one, but should be sufficient for the FluMo detector, as the rate is not so high.

5.2.3 Prototype

During the beam times in April and June 2011, a prototype of the FluMo detector was tested. This prototype consisted out of three BC-404 scintillators, three Plexiglas light guides and three 9111SB photomultiplier including the associated photomultiplier base.

The scintillator was glued to the light guide, using commercially available superglue from UHU (figure 5.15). After gluing both parts together, it was checked that no air bubbles have formed between both parts, so that the light can pass the gluing without being scattered nor reflected. To guarantee the optical contact also from the light guide to the photomultiplier optical grease was used, like for the GIM prototype. For the mechanical support the photomultiplier was fixed to the light guide with several

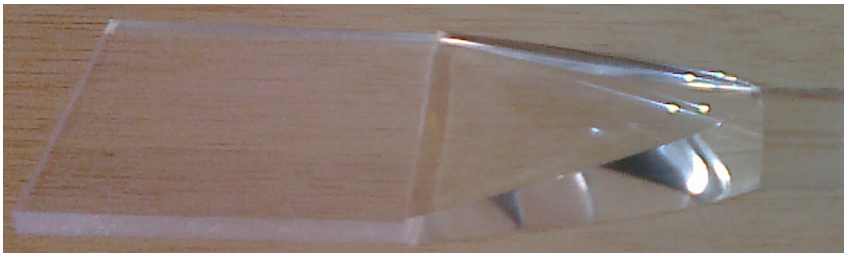

Figure 5.15: The scintillator is glued to the light guide with superglue.

layers of black tape, as it is shown in figure 5.16. This construction proved to be very stable, even for several months.

Figure 5.16: The light guide is attached to the photomultiplier with black tape.

After putting the parts together, everything was covered with light tight black tape and then fixed to a Rose+Krieger profile with a rubber band (see figure 5.17).

Figure 5.17: The prototype of the FluMo detector installed in the experiment, the copper plate was used to test the difference with and without converter.

5.2.4 Final Design

For the final design of the FluMo detector, the scintillators with light guides and the photomultiplier with bases from the prototype were reused. For the housing and proper mounting of the detector, a aluminum tube as housing for the photomultiplier and a holding structure were designed. The goals for the housing and the holding structure were the possibility for easy maintenance, good stability and precise positioning of the detector.

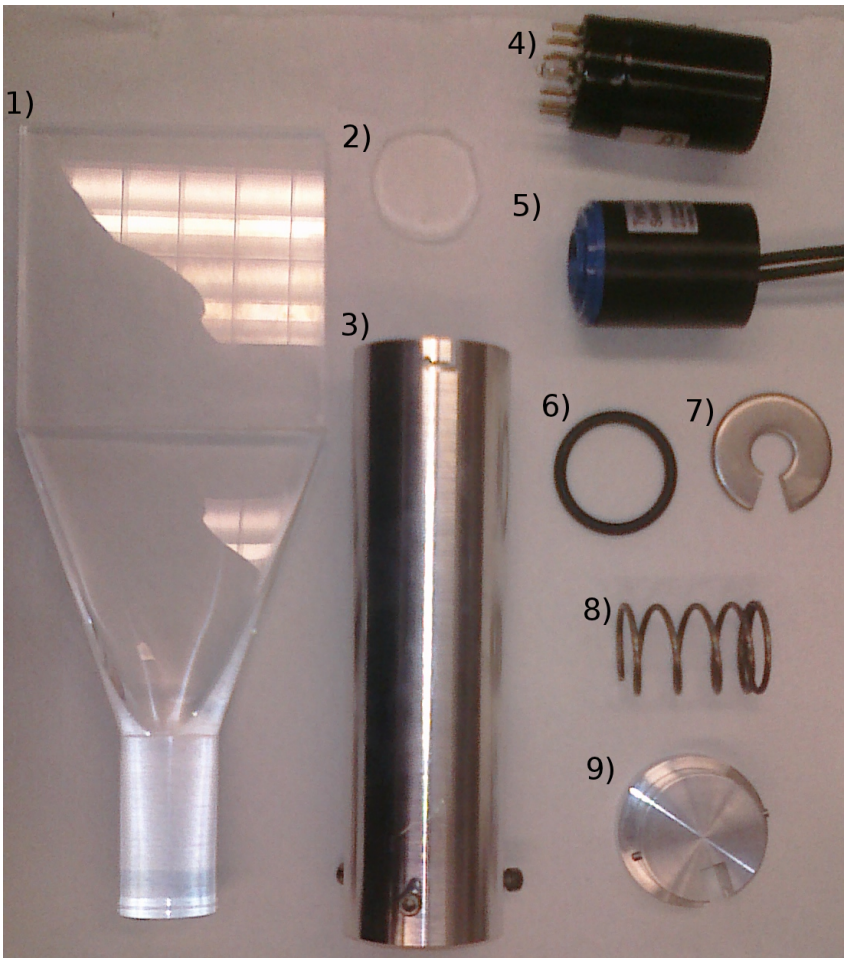

Figure 5.18: The parts, the FluMo detectors are build of.
1) Light guide with scintillator
2) Silicon cookie
3) Housing
4) Photomultiplier
5) Photomultiplier base
6) O-ring seal
7) Steel washer
8) Spring
9) Bayonet cap

The aluminum tube was build on the example of the tagger photomultiplier housings. All parts that were used are shown in figure 5.18. The photomultiplier is connected to the light guide with a silicon

Figure 5.19: All FluMo parts put together in the right order. The O-ring seal guarantees light tightness, the steel washer protects the base from the pressure of the spring.

Figure 5.20: To better guide the photomultiplier in the housing, several layers of tape were added to the front of the photomultiplier.

cookie and isolated against light with a rubber ring at the end of the base. A spring presses on the back of the base, to deliver the needed pressure for a air bubble free connection between light guide and photomultiplier. As the back of the base, where the spring would press on the base, is just filled with silicon, a steel washer was added between both, to apply the pressure to the base housing instead of the silicon (see figure 5.19). Because the photomultiplier has 5 mm diameter less than the inner diameter of the housing, some layers of tape were added to the photomultiplier (see figure 5.20). That way the photomultiplier is centered in the housing, and it can be assured that the photomultiplier has no angle to the light guide. The housing is closed by bayonet cap, so that it can be opened easily for maintenance.

Compared to the tagger, where the housing of the photomultiplier is screwed to the detector housing, the FluMo photomultiplier housing is directly attached to the light guide. As the surface touching the light guide should be as small as possible to disturb the total reflection as little as possible, the housing is fixed to the light guide only by three screws. The alignment of the light guide with the housing is not so easy, but this has to be done only once, so this effort was considered acceptable.

The scintillator and light guide was covered with aluminum foil, to keep the light inside the scintillator and light guide. The optimal way to keep the light inside the material would be a big difference in refractive indexes between the material and the touching material, which for example is the case for air, so that the light will stay inside the material due to total reflection. But as it has to be light tight, the packaging material would touch the surface and therefore disturb the total reflection. Because of this the scintillator and light guide was covered by reflective aluminum foil so that at least most of the light is kept inside. For the light tightness everything was packed into thick, light tight black tape. The three finally assembled FluMo detectors are shown in figure 5.21.

To mount the FluMo detectors in the experiment, an aluminium plate with three holes is used. The aluminum housing of the FluMo detectors fits exactly into these holes and can then be fixed with with a grub screw. Because the housings fit exactly into the holes of the aluminum plate, they are perpendicular on the aluminum plate. After aligning all three in the right distance from the aluminum plate and perpendicular to the beam axis, they can be fixed with the grub screw.

As the holding structure of the FluMo detectors is fixed to the holding structure of the GIM detector, one can align them accordingly to the GIM detector and just align the GIM correctly, which is much easier as the center of the GIM detector is much easier to determine because of its size.

Figure 5.21: Finally assembled FluMo detectors.

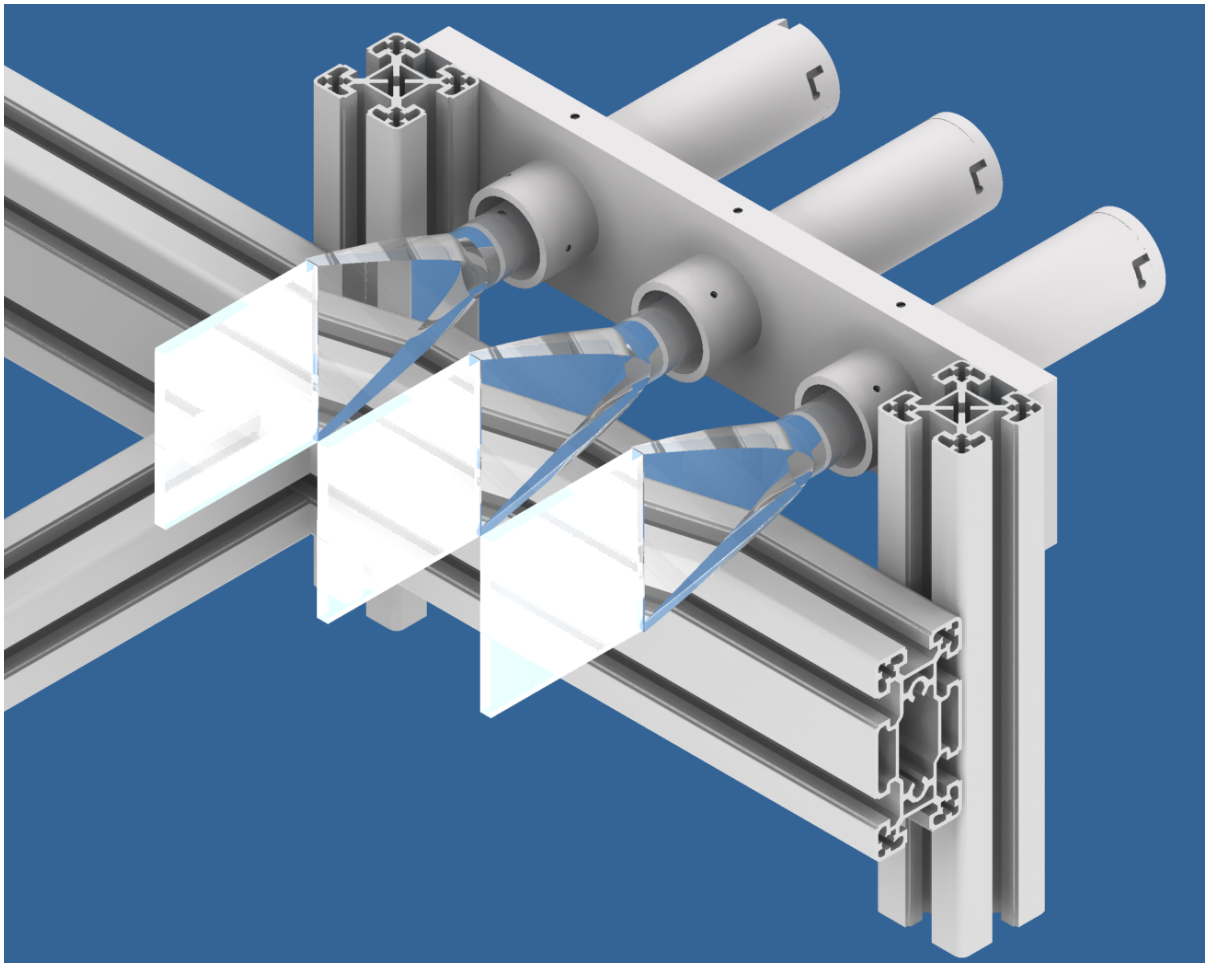

Figure 5.22: Rendered picture of the FluMo detector, mounted on the holding structure.

5.3 Readout Electronics

To process the signals from the photon flux monitor several electronic components are used. The readout electronics is mostly hosted in the TOF rack, beside the experimental area of the BGO-OD experiment, because this is the nearest place to the detector. An advantage of this position is also, that the electronics can be reached while the beam is extracted to the experiment; inside the area or on the electronics platform this would have been impossible. The high voltage for the detector was planed to come from the MOMO/Scifi high voltage. This HV would have had the advantage that one can set a limit for the current and not only the voltage, but because of problems with the electronics ground[8], the high voltage from TOF had to be used.

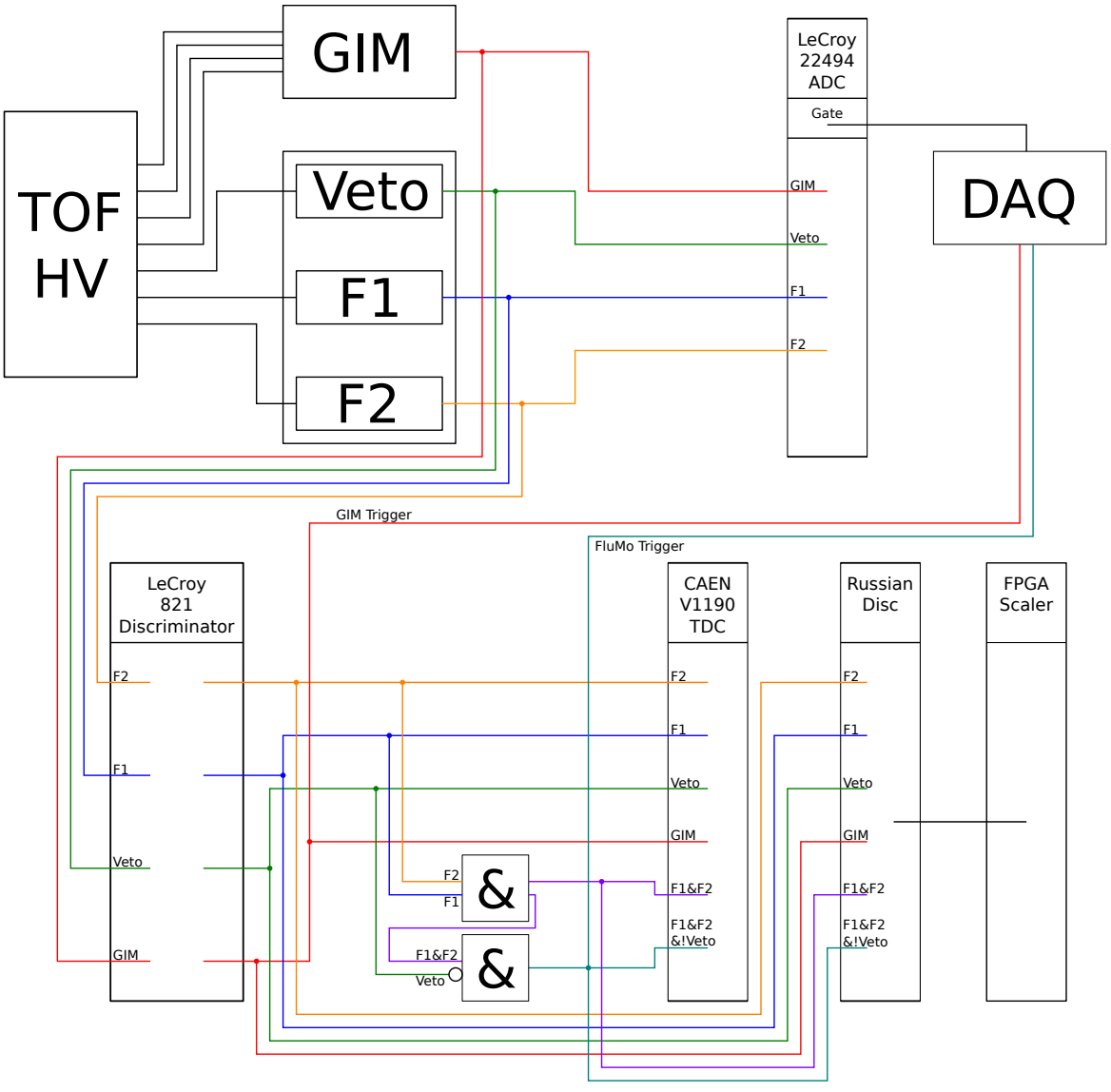

Figure 5.23: Readout electronics for the photon flux monitor.

[8]Because of the large distance between the photon flux monitor and the MOMO and Scifi detector a large loop in the electronics ground was introduced, which caught a lot of noise from the surrounding electronics.

In figure 5.23 an overview of the readout electronics, used during the different test beam times, is given. The signals of all the photomultiplier are split by a splitter. In the April and November beam times active splitter boards [Mes11], and during the June beam time passive splitters were used. The active splitter board has the advantage that, in contrast to the passive splitter, the signal amplitude is not decreased, but the same as the input and one of the two outputs has even an amplification of factor two. A passive splitter would split the signal into to parts, and as it can not generate more charge, the amplitude of the signal is decreased by a factor of two.

One part of the split signals go to a LeCroy 22494 ADC and the other part to a LeCroy 821 discriminator. As the active splitter has the amplified output, the amplified output of the FluMo photomultiplier were used for the ADC, because this increases the resolution of the ADC spectra and makes setting the discriminator thresholds easier. For the GIM photomultiplier the discriminator threshold needs to be very low, so that the amplified output of the active splitter board is used for this.

From the discriminated signals, the coincidences for the FluMo detector are build. One coincidence of the two FluMo scintillators behind the converter and then a anticoincedence of that signal and the signal of the veto scintillator. These two signals and the four signals from the discriminator are then given to a Caen V1190 TDC and FPGA scaler. The scaler is part of the TOF meantimer build by John Bieling [Bie11] and because of the same input as for the TOF-walls has to be used the signals have to go through additional discriminators.

5.3.1 Active splitter boards

The active splitter boards consist out of a passive splitter for the input signal, which reduces the signal size by a factor of two. These signals are amplified by an amplification chip with a bandwidth of 1.7 GHz, which should be enough, even for the short pulses of the GIM photomultiplier. One part of the split signal is amplified by a factor of two and the other part is amplified by a factor of four, so that in the end one signal is as large as the incoming signal and the other one has double the size.

5.3.2 LeCroy 22494 ADC

A ADC returns a digital signal corresponding to the charge of the input signal. The LeCroy 22494 is a 12 channel ADC where one can set pedestal individually for every channel. The pedestal is a offset to the digital output value of the ADC. As the output is always positive, one can move the zero position in the range of positive values by adjusting the pedestal. The ADC integrates all the incoming charge and returns a signal corresponding to this value. As the ADC does not know when a meaningful signal arrives, it needs a gate, that tells the ADC over which time it should integrate the charge of the incoming signal.

5.3.3 LeCroy 821 Discriminator

The purpose of the discriminator is to make a digital signal from the analog one, which timing should be very precise correlated to the timing of the incoming analog signal. The discriminator has a certain threshold, and when an incoming analog signal rises higher than this threshold, an output pulse of fixed amplitude and width is generated.

The LeCroy 821 is a NIM module and has four input channel, where for every channel the threshold and the width of the outgoing pulse can be set with screws. Every channel has five normal and one inverted output. The threshold can be set in a large range from $-30\,\mathrm{mV}$ up to $-1000\,\mathrm{mV}$ and for the output signal a length from 5 ns up to $1\,\mu$s can be set [Fer].

5.3.4 Caen V1190 TDCs

To record the time when an event has happened a TDC is used. A TDC returns the time difference from the trigger time to the last hit. Usually one wants to know the time of all hits that have happened during a given time, so that for this purpose multi hit TDC's are used. A multi hit TDC has a time window in which it save the times of all hits of one channel, and on read out it returns all times within the given time window relative to the trigger time.

The caen V1190 TDC is a multi hit TDC with 128 channels with LVDS input and a VME read out interface. The time window is set to about 3.2 μs and has a resolution of 0.097 656 25 ns. The time window covers the times from about 2.5 μs before the trigger, until about 0.7 μs after the trigger.

5.3.5 Scaler

An other interesting value, especially for the detectors in this work, is the number of events the detector has seen. A scaler is a device that increases a counter by one for every input signal. Because the memory of such an device is not infinite, it resets the counter on every read out, and therefore returns the number of hits since the last read out. To avoid a buffer overflow in the device, it has to be read out in fixed interval.

The scaler used for the read out of the GIM and FluMo detectors are implemented in an FPGA together with the mean timer for the TOF walls [Bie11]. The 32 inputs are sampled with 200 MHz and the count of each input is stored in 31bit counters. To prevent a buffer overflow, the scalers are read out every 50 ms by the data acquisition.

Because this FPGA module is especially made for the TOF walls, it has an LVDS input, which is connected to the discriminators of the TOF wall. To get the signal of the GIM and FluMo detectors to the scaler, they have to be on that discriminator too. This means, that the signal that will be counted by the scaler is discriminated twice. Because of this fact, the signal counted by the scaler has the maximum dead time of the first and second discriminator, which will be visible in the data measured by this scaler.

Additionally there is another scaler (called videoscaler), which counts the trigger inputs for the data acquisition (DAQ). As every hit in the GIM detector and every valid hit[9] in the FluMo detector results in an attempted trigger, the values counted by this scaler can also be used. As the values from this scaler are not influenced by saturation as much as the scaler in the TOF mean timer, the values from the videoscaler are used in this work.

[9] Valid hit means: no hit in the veto, and one hit in each of the other two detectors that were large enough to come over the threshold.

Chapter 6

Detector Tests and Results

After assembling the detectors, they were tested in the laboratory, as well as in the experimental area with beam. In this chapter the different laboratory tests and there results are presented, as well as the results collected during the different beam times in 2011.

6.1 Laboratory Tests

In the laboratory every detector was subjected a test of general functionality. A test with cosmic particles was done, to test if the detector can see a particle at all. This test was done to assure general functionality of the detector and it's components. With theses test, e.g. a not working base of one of the FluMo detectors was found.

Additionally the photomultiplier of the FluMo and GIM detectors were tested for it's rate stability, and the FluMo detectors were also tested for their efficiency.

6.1.1 GIM photomultiplier rate stability test

For testing the rate stability of the photomultiplier, reproducible light pulses had to be produced. For this purpose a diffuse green standard LED was pulsed with a Agilent 33250A function generator. The pulse given to the LED had an amplitude of 3 V and a pulse length of 8 ns with a rise and fall time of 2.5 ns which is the minimum the function generator can produce. The LED was pointing in the direction of the photo cathode of the photomultiplier, positioned in the middle of the photomultiplier window and as near as possible, so that as much light as possible reaches the photo cathode. The high voltage supplied to the base was 1600 V and in the case, the booster was turned on 196 V was applied to the first booster and 435 V to the second booster. The used high voltage power supply (iseg T3DP 030 405 EPU) also provided a display to measure the current flowing through the photomultiplier base. The observed signal height was measured with an LeCroy WaveAce 224 oscilloscope with persistence set to infinity and then read the average from the scale. The errors were guessed by the width of the distribution of signals in the persistence view.

The results of this test are shown in figure 6.1. The test was done with a base, like it is used in the TOF walls and with the booster base of the GIM prototype. For the booster base one test without connected booster and one test with two booster connected was done. No test with all three booster connected was done, as the used power supply had only three outputs available.

For the TOF base, which was the model the GIM base was designed after, one can see that the signal amplitude increases with the rate until a peak at about 7 MHz and then steadily decreases. The decrease of the Amplitude, after the peak, is due to the current flowing through the voltage divider is in the order of current flowing through dynodes, which causes a drop in the amplification, like explained in section 5.1.3. The increase of the Amplitude could be due to the base line shift, which is illustrated in figure 6.2. The pulse of a photomultiplier is not like an ideal digital signal, with zero rise and fall time, but has

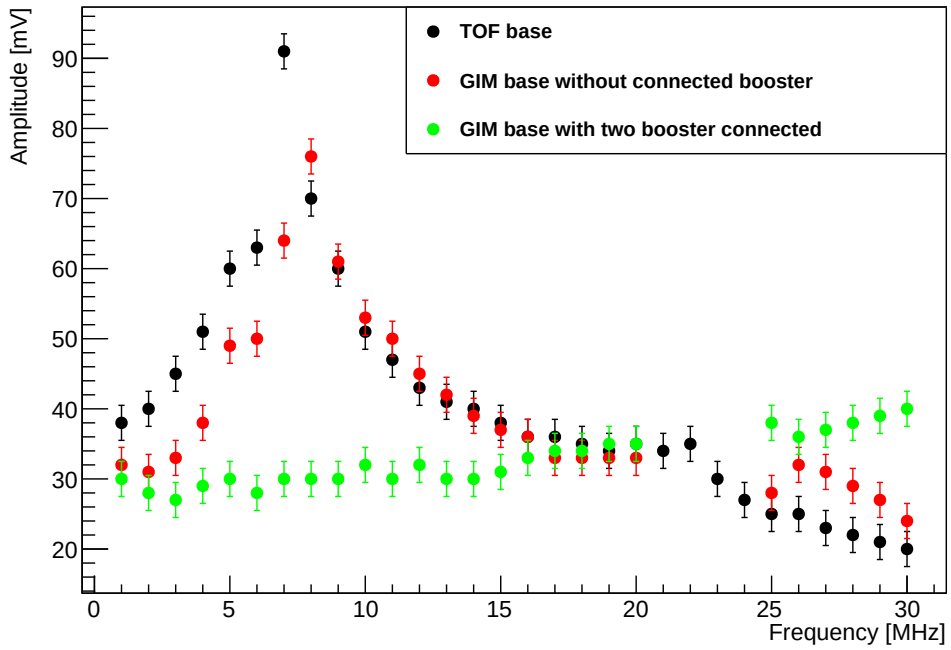

Figure 6.1: Results of the LED pulser test, for different bases and connected booster of the GIM photomultiplier.

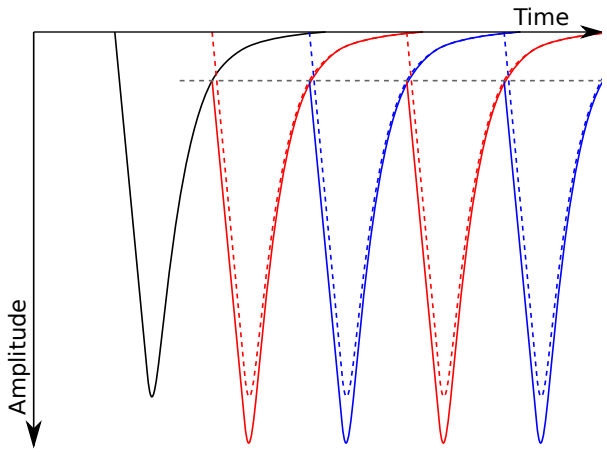

Figure 6.2: Baseline shift, the red and blue pulses do not start at 0 mV but with a certain offset, which is caused by the previous pulse. The "shifted" baseline is marked in gray.

a short rise time and a bit longer, exponential fall time. When the next arrives before the previous pulse is completely decayed, it adds another amount of amplitude on top of the amplitude from the previous pulse. When this happens for several pulses everything looks normal, but all pulses have an offset. Due to this effect one can see pulses, even when they would be under the threshold in normal conditions. But this effect should occur only for higher frequencies, so that this effect is not understood, but as this

effect does not occur with the boosters connected to the booster base used for the GIM detector I did not care about it.

The new GIM base, without any booster connected, is electrically the same as the TOF base. Due to a tolerances in the resistor and capacitor values, one can see small deviations from the TOF base, but in principle they are behaving the same. One can see the same peak in the amplitude and for higher frequencies the steadily decreasing amplitude. With two booster connected, the picture changes completely. Over all frequencies up to 30 MHz no drop in the amplitude can be seen, just a slightly increasing amplitude which in this case looks very much like the baseline shift.

I also tried higher frequencies, but as the pulses of the LED were to broad these results were considered not realistic. But what was observed during these tests is, that when the amplitude of the photomultiplier with attached boosters decreases, this was always caused by the current limit of the high voltage power supply. If the booster at the last dynode of the photomultiplier needs more current than the set limit of the power supply, the amplitude drops immediately. Because of this the main limitation for the rate stability of the GIM photomultiplier will be the supplied current at the last dynode. Which means that for the maximum rate stability the gain of the photomultiplier should be chosen as small as possible.

6.1.2 FluMo efficiency test

The FluMo detectors need an efficiency of 100% for electrons. To prove this, the following test was performed. As source for electrons, a strontium-90 source was used and laid on top of the scintillator to test. As a trigger a second FluMo detector was used and laid under the tested one. The discriminator signal of the detector to test was given to a gated scaler and the discriminator signal of the trigger detector was given as the gate. As reference, this signal was also given to a scaler, so that one could compare the number of hits seen by every detector.

The assumption for this test is, that every hit in the detector to test, come from a particle form the source, which has to pass the detector to test, before it is recognized in the trigger scintillator. This assumption is not correct, as also cosmic particles can hit the trigger scintillator, but not the scintillator to test. This could have been solved by adding a second trigger detector in front of the detector to test, and only count particles that have passed both detectors. But this is not possible, because the electrons from the strontium source are stopped within two of the FluMo scintillators.

Detector	Counts	Reference Counts	Efficiency
FluMo Veto	207517	201213	97.0 ± 0.3%
FluMo 1	317447	300450	94.6 ± 0.3%
FluMo 2	228691	218807	95.7 ± 0.3%

Table 6.1: Results of the efficiency measurement of the FluMo detectors

In table 6.1 the results of this test are shown, with statistical errors given for the efficiency. As one can see the efficiencies are in the range of about 94% – 97% which is not the 99.9% efficiency that was expected from these scintillators. But because the test configuration was not very good without a third detector one can expect the result to be a bit worse than expected. Also the results from the test during the beam time (section 6.2.2) look much better.

6.1.3 FluMo photomultiplier rate stability test

The FluMo photomultiplier was tested in a similar way to the GIM photomultiplier. The test was performed only with the C673ASN2 base, but with different voltages. Instead of the LeCroy oscilloscope, a MSO 5104 from Tektronix was used, and the measurement points were got with its measurement functionality. As amplitude the mean amplitude and as error the standard deviation of 500 measurements are plotted in figure 6.3, for 1000 V, 1100 V and 1200 V.

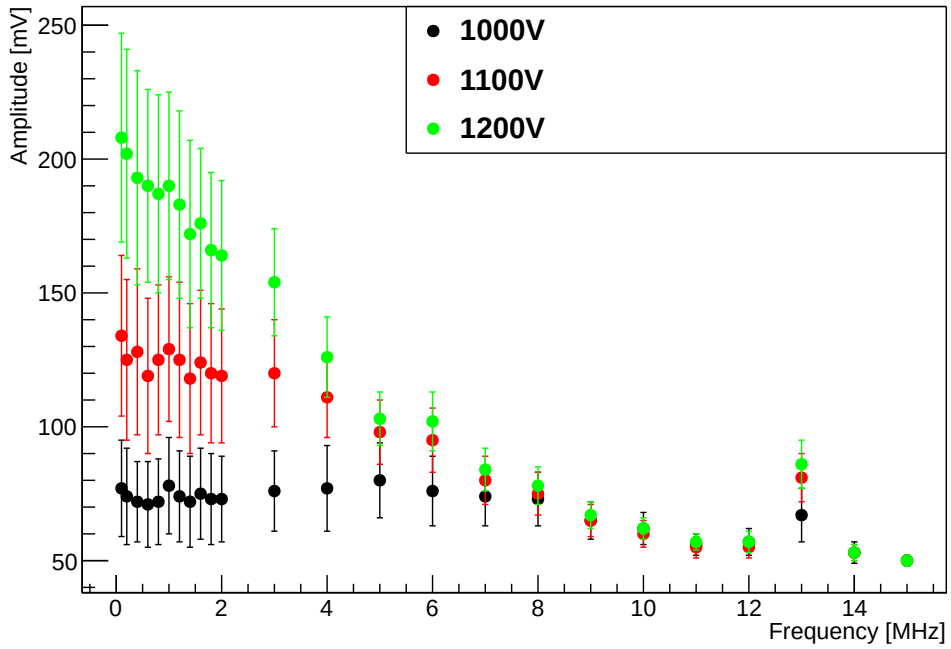

Figure 6.3: Results of the LED pulser test of one of the FluMo photomultiplier.

At 13 MHz the amplitude of the signal increases for all applied high voltages. This is caused by the LED, which produces more light at just this frequency. With another Photomultiplier it has been verified that the LED is emitting more light and that this is not an effect of the photomultiplier itself. But this also indicates, that this measurement is not independent on the LED. Some part of the observed behavior can be caused by effects of the LED. But because the amplitude for all high voltages arrive at 50 mV in the end, this is not caused by the LED, but caused by real saturation effects of the photomultiplier, most probably the limited current that can flow through the voltage divider, which causes a drop of the amplification at the last dynodes of the photomultiplier.

What we can see from this measurement is, that with lower high voltage the amplitude of the photomultiplier signal is stable up to higher rates, than for a higher high voltage. For 1000 V of high voltage the amplitude does not drop down until about 8 MHz, whereas for 1100 V an decrease of the amplitude can be observed already at 3 MHZ and for 1200 V even no plateau with a constant amplitude is visible. Therefore the high voltage setting of this photomultiplier should again be as small as possible, and not more than 1000 V. But as I also observed during this test, that I won't get good signals with high voltages lower than 1000 V, this voltage is the one one should use during the experiment.

6.2 Beam Tests

Additionally to the tests in the laboratory, the photon flux monitor was also tested during three test beam times in its final position in the experiment. During the test beam times in April and June the prototype detectors were used and during the test beam time in November and December, the final detector designs were used.

During the test in the experimental area, one big problem occurred that was not existing during the test in the laboratory: the much higher noise level. In the laboratory the noise level was nearly zero and it was no problem to detect signals with an amplitude of 40 mV; in the experimental area, this was completely different. Due to a lot of other electronics, the electronics ground was oscillating with an amplitude of up to 30 mV. Because the signals of the GIM detector should be as small as possible, to guarantee a high count rate stability, this amount of noise was really problematic.

Because of the oscillations, the threshold is not the same for every signal. Due to the oscillations the signal can have an offset of up to 30 mV, which is as large as the minimum threshold of the used discriminator. This is especially a problem for the ADC's, because it is sensitive to the area below the signal, and this is dramatically increased with the offset.

But for the last beam time in December the noise was reduced by a factor of two, by changes to the distribution of the electronics ground for the whole BGO-OD experiment. After this and using an additional four times amplifier for the GIM detector, that was mounted between the photomultiplier and the active splitter the problems caused by this noise were still visible but much smaller.

6.2.1 Rate stability

To prove the rate stability of the detector, the numbers counted by the detectors have to be compared to the real number of photons; but the real number is unknown. Therefore the counted numbers have to be compared to values that are proportional to the real number of photons, and are not affected by saturation effects. One detector that counts a proportional number is the tagging detector. But also the tagging detector can saturate, so that it could be hard to interpret the results. A solution for this problem is to use only the bars of the tagging detector where the electrons are recognized, which have transferred most of there energy to the bremsstrahl photon. Because the probability of transferring a lot of energy to a photon is much lower than transferring only a small amount of energy there are much more low energy photons and therefore high energy electrons. The tracks of these high energy electrons will be bend by the magnetic field of the tagging magnet much less than the low energy electrons that have produced high energy photons. Therefore the rate in the tagger bars that recognize the low energy electrons is much lower than the rate in the bars detecting the high energy electrons. Because the shape of the bremsstrahl spectrum is independent on the rate of the incoming electrons, the rate from the bars for the low energy electrons is proportional to the rate of the total tagger.

Another possibility to check the rate stability, is to compare the extracted current from the accelerator with the rate in the detector. But only if the bremsstrahl target does not change! To proof this relationship in figure 6.4 the extracted current from ELSA is plotted against the scaler rate of the OR of the six lowest tagger bars, which detect the electrons with the lowest energies, measured by the videoscaler during the November 2011 beam time. One can see in that figure a nice linear dependency between both values. Because of this result I will compare the rates of the photon flux monitor only with one of both values. The values of the current extracted from ELSA are spreading a lot, and comparing runs with different bremstrahl targets wouldn't be easy, so that I choose the rate of the lowest six tagger bars as reference value.

Form figure 6.5 one can see how it looks like, when one of the compared detectors goes in saturation.

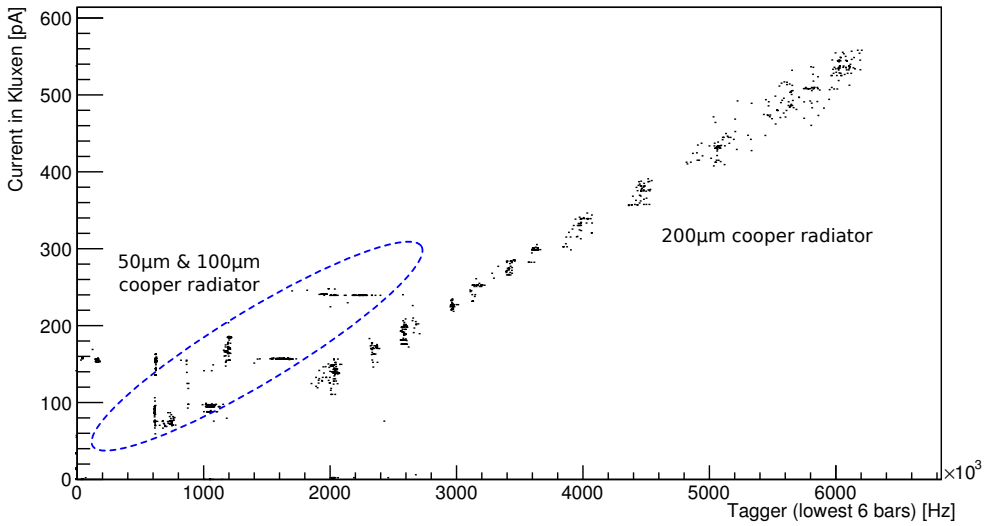

Figure 6.4: Current from ELSA extracted to the BGO-OD experiment compared with the rate of the lowest six tagger bars. The values are from the beam time in November.

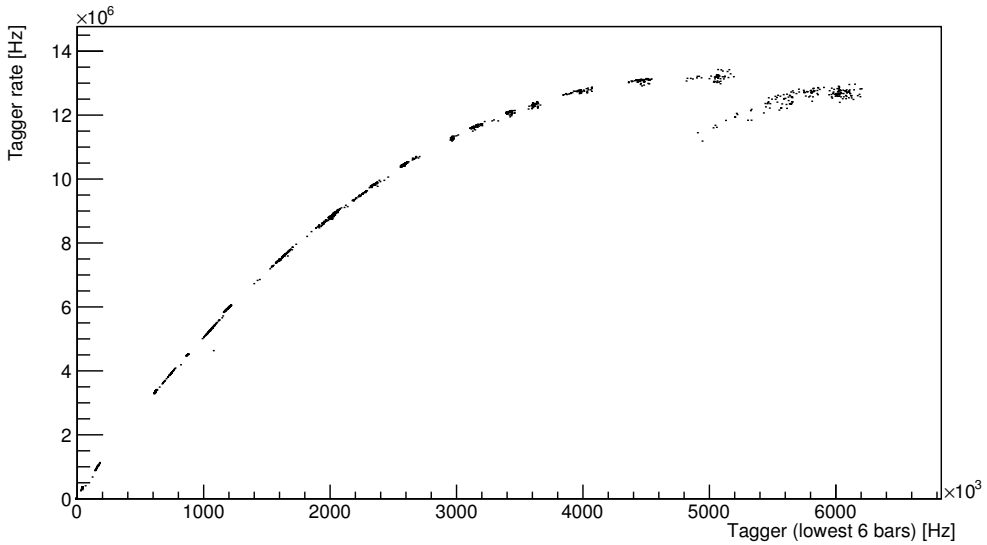

Figure 6.5: Rate in the total tagger compared with the rate of the lowest six tagger bars

In this case the count rates of the lowest six tagger bars are compared to the count rates of the total tagger measured by the videoscaler during the November 2011 beam time. Starting from a rate of 6 MHz in the total tagger, the line starts bending towards the axis of the lowest six tagger bars, which means that the rates are no longer proportional to each other, so that one of them saturates. As the line bends towards the lowest six bars the upper bars of the total tagger have to be in saturation. In this plot is also an other effect visible: the entries with the highest rates are not on the same line as the other values. As for every

rate the settings of the accelerator needs to be changed and it was started with the highest rates, it seems that the beam was not completely stable during this time.

Because in all the following graphs the rate in the lowest six tagger bars is used as a reference, one has to multiply this value by the slope of a linear slope fitted to the lower part of graph in figure 6.5 to get the rate seen by all tagger bars. This linear slope is not shown in the figure because of clearness, but a linear fit to the values from 0 MHz to 1 MHz of the lowest six tagger bars gives a slope of 5.6, so that one has to multiply the value from the lowest six tagger bars by 5.6 to get the rate seen by the total tagger.

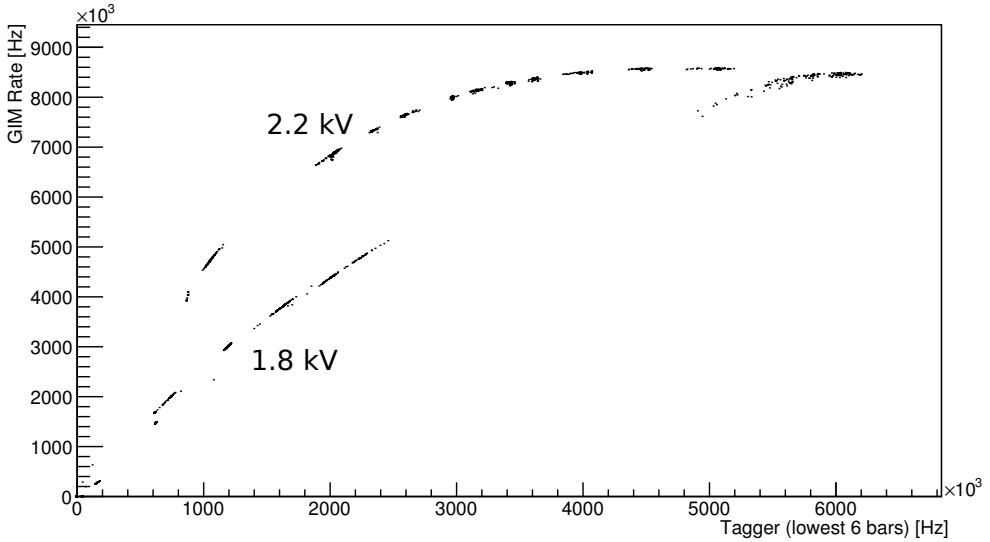

Figure 6.6: Rate in the GIM detector compared with the rate of the lowest six tagger bars

In figure 6.6 the same runs as before are plotted for the count rate of the GIM detector against the lowest six tagger bars. Also in this figure one can see the artifacts at the highest count rates. In the GIM diagram are also two lines visible, which appear due to different high voltage settings, and therefore different gain of the photomultiplier. From these lines one can clearly see the impact of higher high voltages on the rate stability of the detector. Due to the higher high voltage, the pulses from the photomultiplier are bigger (as desired by the higher high voltage) and because of this, the current flowing through the photomultiplier also increases. Because of this, the high voltage power reaches its current limit much earlier and the booster of the last dynode of the photomultiplier can not provide as much current as needed. If not enough current is available, the amplitude of the resulting pulse of the photomultiplier will be smaller and the pulse will not be recognized by the discriminator. This means that the detector can reach a much better rate stability, just by lowering the supplied high voltage. Of course, lowering the high voltage has the disadvantage, that the gain of the photomultiplier is lower and therefore a lower discriminator threshold is needed.

For 2.2 kV curve the saturation starts at about 0.8 MHz of the lowest six tagger bars, which corresponds to about 4.5 MHz in the total tagger and for the lower high voltage the saturation starts at 1.2 MHz in the lowest six tagger bars which corresponds to about 6.7 MHz in the total tagger. Therefore one can conclude that the GIM measures the rate correct at least up to 4 MHz.

In figure 6.7 the rate in the total FluMo detector, which means no hit in the veto detector but one hit

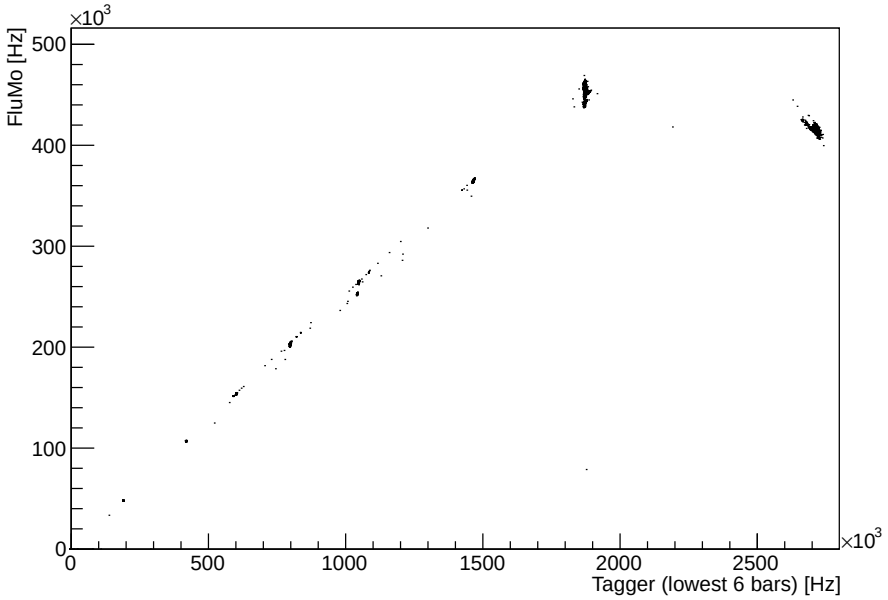

Figure 6.7: Rate in the FluMo detector compared with the rate of the lowest six tagger bars

with the right pulse height in the both of the other two scintillators, is plotted against the rate in the lowest six tagger bars. Because the FluMo detector was not working properly during the November beam time, this measurement was done during the beam time in December 2011. One can see a very straight line up to 1.8 MHz where the saturation starts and the count rate does not increase further, which corresponds to a rate in the total tagger of about 10 MHz. This is not the desired rate of 50 MHz one wants to achieve, but this increases the range where the GIM detector measures correct results by a factor of two. Also it is possible to improve the rate stability of the FluMo detector in the future.

To calculate the fraction of photons the FluMo detector is counting, the data plotted in figure 6.8 can be used. In this plot the rate measured by the GIM detector is plotted against the rate measured by the total FluMo detector. Due to a linear fit to the lowest rates it is possible to determine the fraction photons counted by the FluMo detector. A linear fit to the points up to 120 kHz in the FluMo detector one gets a slope of 75.0 ± 0.1. So that multiplying the rate measured by the FluMo by 75.0 gives the total number of photons that would have been seen by the GIM detector if it would not have been in saturation.

In figure 6.8 also some outlying points are visible. During the beam time in December 2011, when these values were measured, different settings for the GIM detector were tried which then caused different count rates that can be seen in as outlier in this plot.

6.2.2 Efficiency

Determining the efficiency of the detectors, just by the test beam data, is not so easy. To prove the efficiency of an detector, one has to know when a particle has crossed the detector. Therefore one usally installs one detector in front and one detector behind the detector to test. When a particle is recognized in front and behind the detector, the particle must have crossed the detector. During the beam time no additional detectors were installed, so the existing ones had to be used for this test. But due to the different purposes of the different detector parts, they have different thresholds. The FluMo 1 and

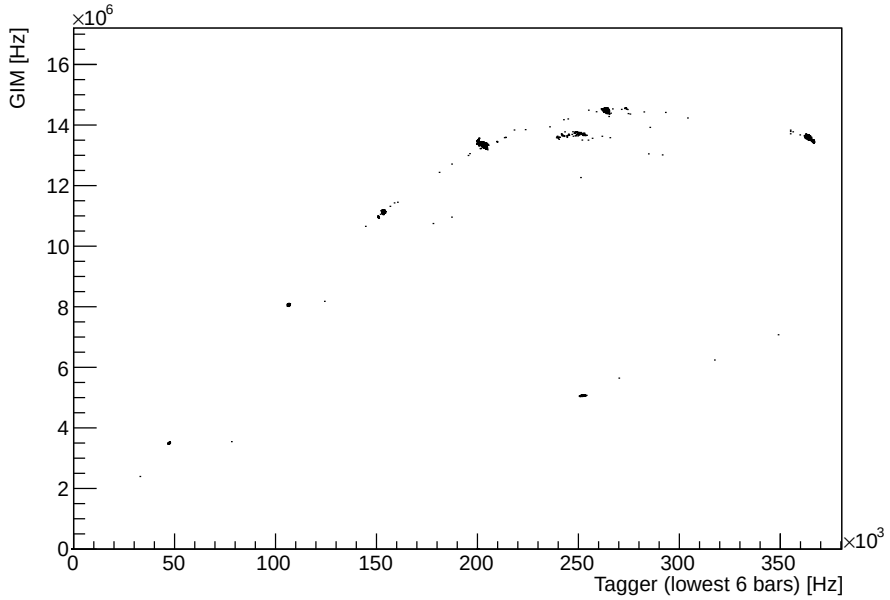

Figure 6.8: Rate in the FluMo detector compared with the rate of the GIM detector

FluMo 2 detectors have to count only if the energy of two minimal ionizing particles was deposit in the detector, so that these detectors won't count single electron events. But when calculating the efficiency, the single electron events were taken into account too, because they were seen by the detector in front and behind, the resulting efficiency has to be less then 100%. Therefore the efficiency of the FluMo 1 and 2 detectors in this test is much less then 100%.

To test the efficiencies of the different detectors, hits in different detectors were required. For the efficiency calculation of the FluMo veto detector a hit in the tagger, FluMo 1, FluMo 2 and GIM was required, for the FluMo 1 a hit in the tagger, FluMo Veto, FluMo 2 and GIM, for the FluMo 2 a hit in tagger, FluMo veto, FluMo 1 and GIM and for the GIM a hit in tagger, FluMo veto, FluMo 1 and FluMo 2 was required. So that for every detector a hit in front and behind the detector was required, expect for the GIM detector, where it was assumed that if a particle is detected in the tagger and all FluMo detectors it has enough energy to also arrive at the GIM detector.

In figure 6.9 efficiencies of the different detectors are plotted against the tagger bar, where the electron was detected, which produced the photon. As expected the efficiency of the FluMo 1 and FluMo 2 detectors is lower, as they are configured to count only hits of two minimal ionizing particles. But even if the efficiency of these two detectors would really be lower, it would be just an additional factor that is multiplied to fraction of photons the FluMo detector is counting. For the functionality of the FluMo detector only the efficiency of the veto detector is important and this efficiency is larger then 99.6% and no dependency on the photon energy is visible. For the GIM detector an efficiency of about 97%, independent of the photon energy, was measured. Which is less then the required efficiency of more then 99.9% and is most probable caused by the radiation damage which is described in section 6.2.4. Due to the radiation damage the transmission of the detector material is decreased, which means that the light produced due to the Čerenkov effect is absorbed and can not be recognized by the photomultiplier, so that this point needs some improvements.

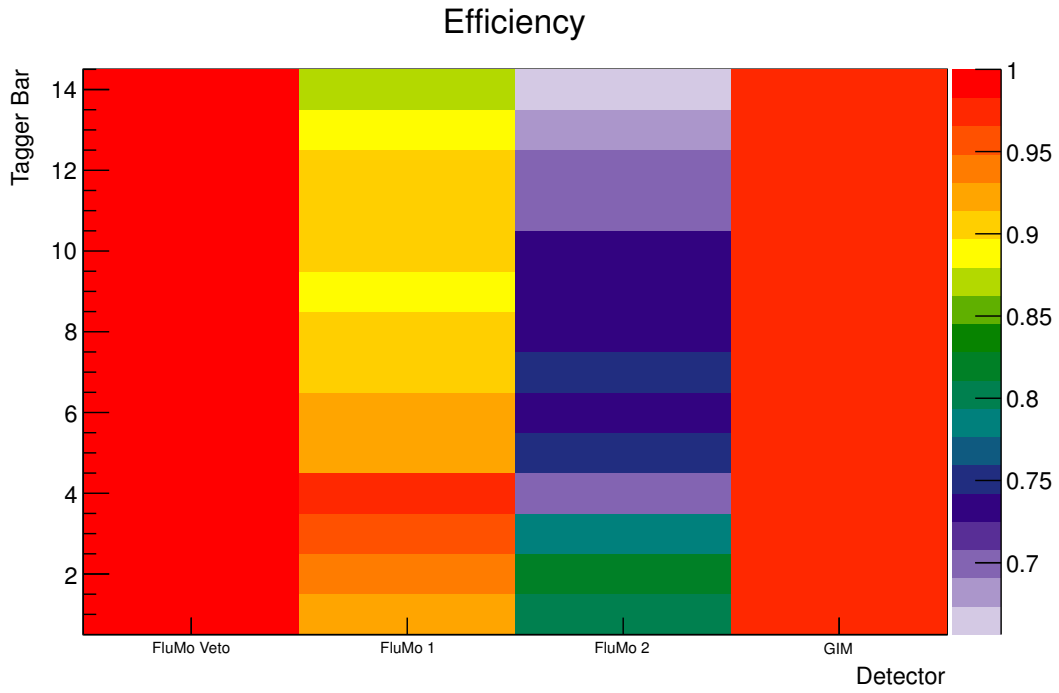

Figure 6.9: Efficiency of the different FluMo detectors and the GIM, plotted against the the tagger bar where the corresponding electron was recognized. (Projections of this plot for every detector part can be found in the appendix)

6.2.3 Energy resolution of the GIM detector

Because the GIM detector is an absolute absorption detector, all the energy of an incoming particle is deposit in the detector material. As the light output of the detector material is proportional to the deposit energy, one can get the amount of deposit energy from the pulse size. With the ADC acquisition this information is available and can be evaluated.

The deposit energy is an interesting value, because one wants to have all those photons that are tagged by the tagger. As the tagger tags a certain range of energy, it is possible to compare the energies in both detectors (GIM and tagger) and set the threshold of the GIM detector accordingly to the lowest photon energy tagged by the tagger.

In figure 6.10 the raw ADC entries of the GIM for one run are plotted against the tagger bar, where the electron, which is associated to the photon detected in the GIM, is detected. For this plot, only ADC entries were used, where only one tagger bar were hit and where an entry in the GIM TDC is existing. Due to the earlier mentioned noise, the the values for one tagger bar spread over 100 ADC channels. But when one has a close look, one can see that the entries of the lower tagger bars, where the electrons according to the high energies are recognized, the values are a little bit higher than for the upper bars, where the lower energies are recognized. When one looks just at the mean ADC values per tagger bar, which is shown in figure 6.11 one can clearly see a linear dependence between the tagger bar and the mean energy deposit in the GIM. But the difference between the lower and the upper tagger bar corresponds to only 50 ADC channel in the GIM, which is only half of the spread caused by the noise.

This proves, that the signal size of the GIM detector is correlated to the energy of the incoming particle, but this is not useful to set a threshold that corresponds to the energy range tagged by the

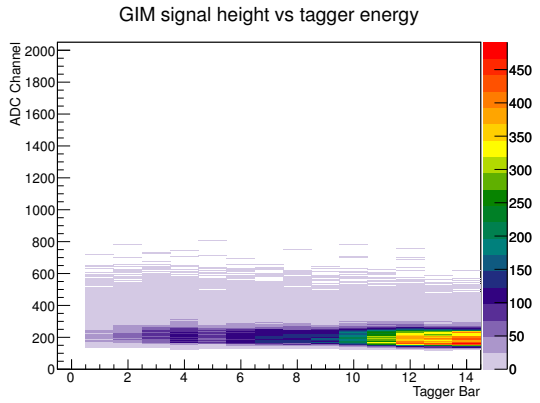

Figure 6.10: Energy detected by the GIM detector against the tagger bar, the according electron was recognized.

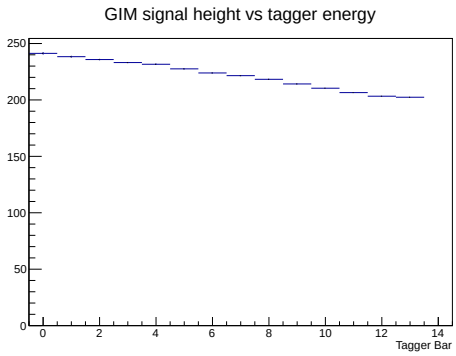

Figure 6.11: Mean values of the energies detected by the GIM detector per tagger bar, the according electron was recognized.

tagger. But for this purpose the plot from section 6.2.2 might be more useful. One has to set the threshold that the efficiency of the most upper bar just reaches it's maximum.

6.2.4 Radiation damage of the GIM detector material

As already mentioned in section 6.2.2, the lead glass of the GIM detector is affected by radiation damage. Due to the high energy deposition in the crystal the lattice structure is changed in a way that it is not transparent anymore. But the transparency should increase on its own after some time without irradiation and it should be possible to restore the the transparency by treating the lead glass with ultra-violet light or heat.

I have tried to restore the transparency of the lead glass block of the final GIM detector by treating it with UV-light. As light source a mercury vapor lamp was used and the detector material was illuminated in the direction of the photon beam of the experiment. But after a illumination time of more then 60 hours no change in the transmission was visible. According to [Ach01] more then 90% of the transmission should have been restored after this time of irradiation, which should have been clearly visible even without any measurement.

Figure 6.12: Lead glass of the GIM prototype after the irradiation.

That the transparency could be restored was observed from lead glass of the prototype. In figure 6.12 the lead glass of the GIM prototype is shown after the irradiation through the photon beam and in figure 6.13 the same lead glass is shown 60 days later. As one can see from the images the transparency was restored by a large amount during this time. Of course the settings for both pictures are different, so that

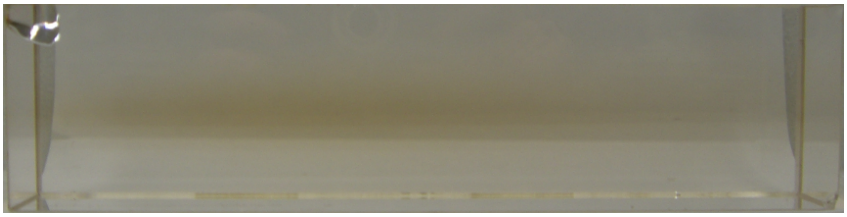

Figure 6.13: Lead glass of the GIM prototype after 60 days in the laboratory.

one can not conclude exact values from these pictures, but the pictures reflect the optical impression of the restoration of the transparency. After 60 days of illumination through sunlight through windows and light from fluorescent tube lamps, as well as storage at room temperature the transmission of the lead glass was restored nearly completely.

Therefore it should be possible to speed up this process, but it seems that the intensity of a simple mercury vapor lamp is not enough, so that one has to think about a better solution for the future.

Chapter 7

Conclusion and Outlook

The goal for the Photon Flux Monitor of the BGO-OD experiment were defined in section 4.2: Count rate stability for rates up to 50 MHz. As the photon flux monitor was divided into two parts, the requirements for the GIM detector were an efficiency of 100% and count rate stability for lower rates. The goals for the FluMo were a count rate stability for rates up to 50 MHz.

GIM

In section 6.2.1 and 6.2.2 the count rate stability and the efficiency of the GIM detector were tested. Whereas the count rate was proofed to be stable up to a tagging rate of at least 4 MHz, the efficiency of the detector couldn't be proofed to be 100%. Because of the lower efficiency, the detector is not counting every single photon, but only about 97% of the photons. So that this factor needs to be considered in the calibration of the FluMo or needs to be improved in the future. As this problem is most probably caused by the radiation damage, which couldn't be proofed during the theses, solving the radiation damage problem can also increase the efficiency of the GIM to the desired 100%.

FluMo

The count rate stability of the FluMo detector was tested as well in section 6.2.1. This test has proven that the rate measured by the FluMo detector is proportional to the lower rates measured by the GIM detector and also to the rate measured by the tagging detector up to 10 MHz. Therefore the goal of count rate stability of up to 50 MHz has not been achieved, but compared to the GIM detector the range has been improved. Probably this range can be improved in the future by modifying some parts of the FluMo detector.

7.1 Outlook

For the near future a solution for the radiation damage of the GIM detector needs to be found. There are two possibilities to solve this problem. The first possibility is to use the GIM detector only for a short amount of time at the beginning of a beam time, when the lead glass is still undamaged, and calibrate the FluMo. After the calibration the GIM detector will then be moved out of the beam, so that no further damage happens to the lead glass. Optionally the radiation damage that occurred during the calibration can be healed with UV-light. The second possibility would be to make a new version of the GIM detector with another detector material. The GIM detector of the CB experiment uses PbF_2 crystals and there no radiation damage was observed while it was rebuild in 2008 [McG08]. Because of this and the results from A4 experiment [Ach01], where it was found that the radiation hardness of PbF_2 is 10 times higher then the one of lead glass, I assume that changing the lead glass against a PbF_2 crystal would solve the radiation damage problem. This solution would also have several other advantages, that the GIM

detector can be used for other studies too. For example it is possible to get the collimated bremsstrahl spectra, when one requires in addition to a hit in the tagging detector a hit in the GIM detector.

The next point for future enhancements of the photon flux monitor, would be to expand the count rate stability of the FluMo detector up to the desired rate of 50 MHz. To achieve this, the photomultiplier - base combination of the FluMo detector needs to be improved. The first step would be to exchange the existing passive bases with active bases as described in section 5.1.3 for the GIM detector. If this is enough to expand the range of stable count rates up to 50 MHz needs to be investigated.

It would also be possible to use the detectors of the photon flux monitor for other measurements, then they were designed for. One possibility was already mentioned: the possibility to get collimated bremsstrahl spectra, when requiring a hit in the GIM detector for the bremsstrahl spectra. Because only photons that have passed the collimator can be recognized in the GIM detector, the resulting spectrum is a collimated one. Another possibility would be to calculate the thickness of the used target with the FluMo detector. Instead of using the veto detector as a veto, but requiring a hit in the detector, the FluMo counts all electron-positron pairs that were produced in front of the FluMo detector. If one makes a measurement with and without, or with a full and a empty target one can get the number of electron-positron pairs that were produced in the target. And from that value and the total number of photons it is possible to get the length of the target in radiation lengths. As the radiation lengths is a known property one can calculate the actual length of the target.

Appendix A

Appendix

A.1 GIM booster base PCB layout

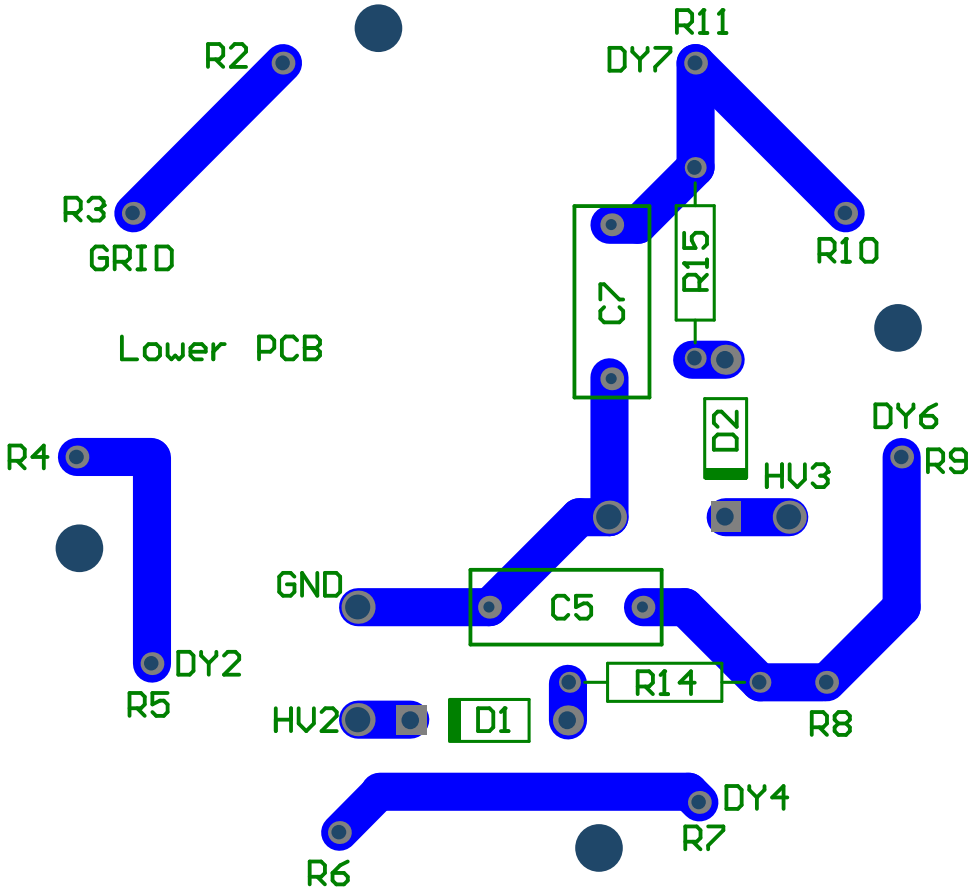

Figure A.1: PCB Layout for the upper PCB of the GIM booster base

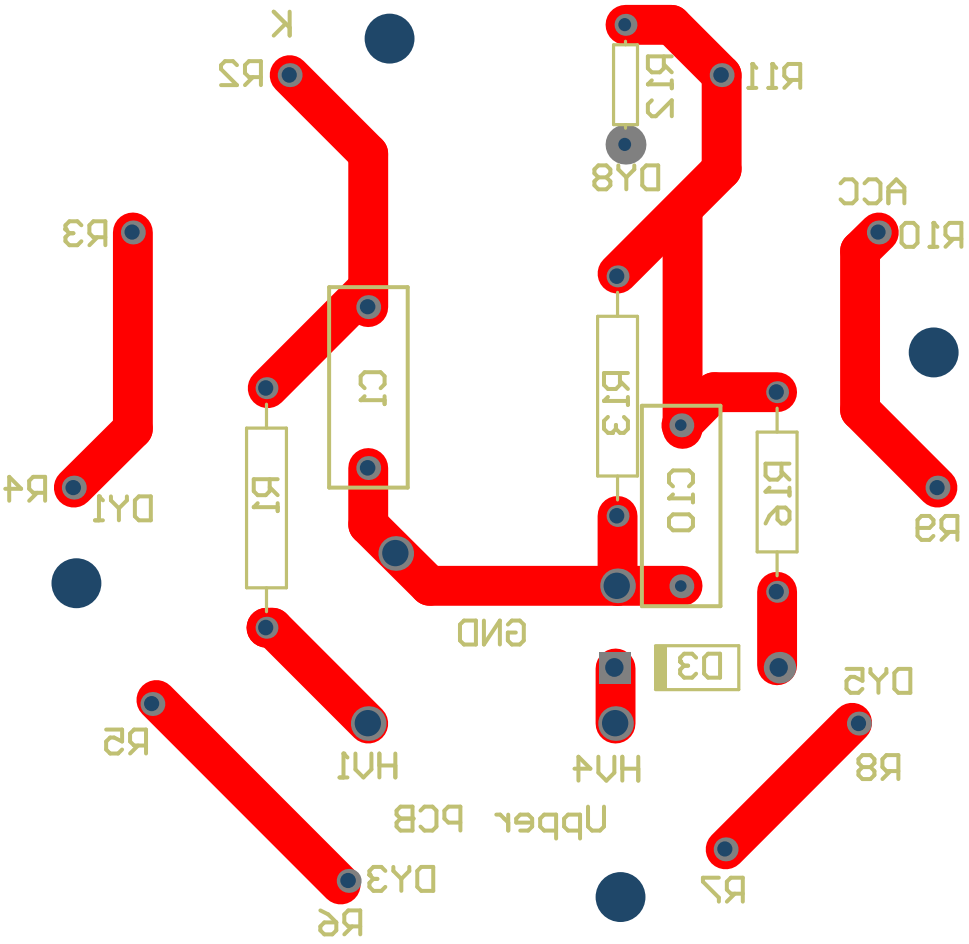

Figure A.2: PCB Layout for the lower PCB of the GIM booster base

A.2 Technical drawings of the housing for the GIM base

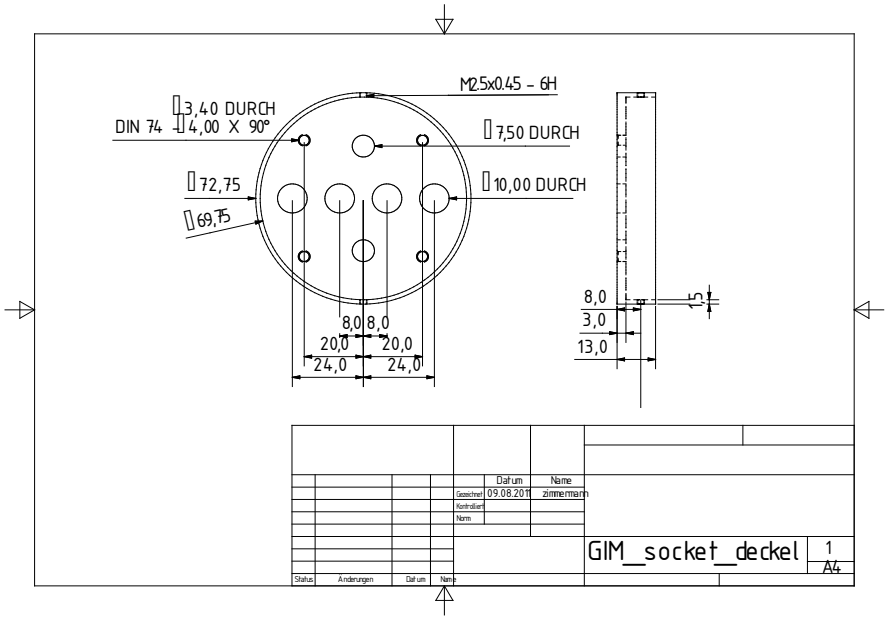

Figure A.3: Cap of the housing of the GIM base

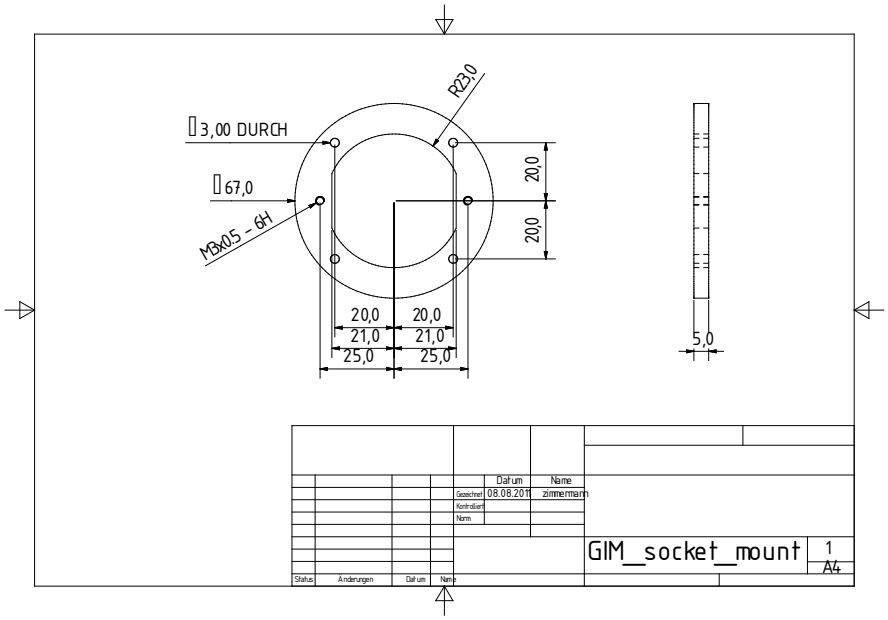

Figure A.4: Bottom part of the housing of the GIM base

A.3 Technical drawings of the FluMo housing

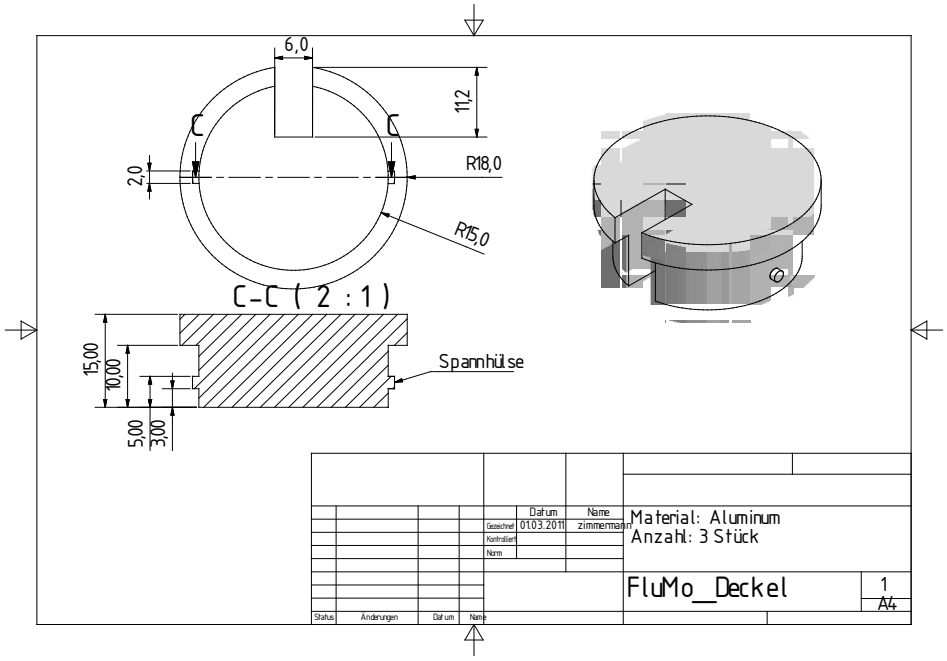

Figure A.5: Bayonet cap of the FluMo housing

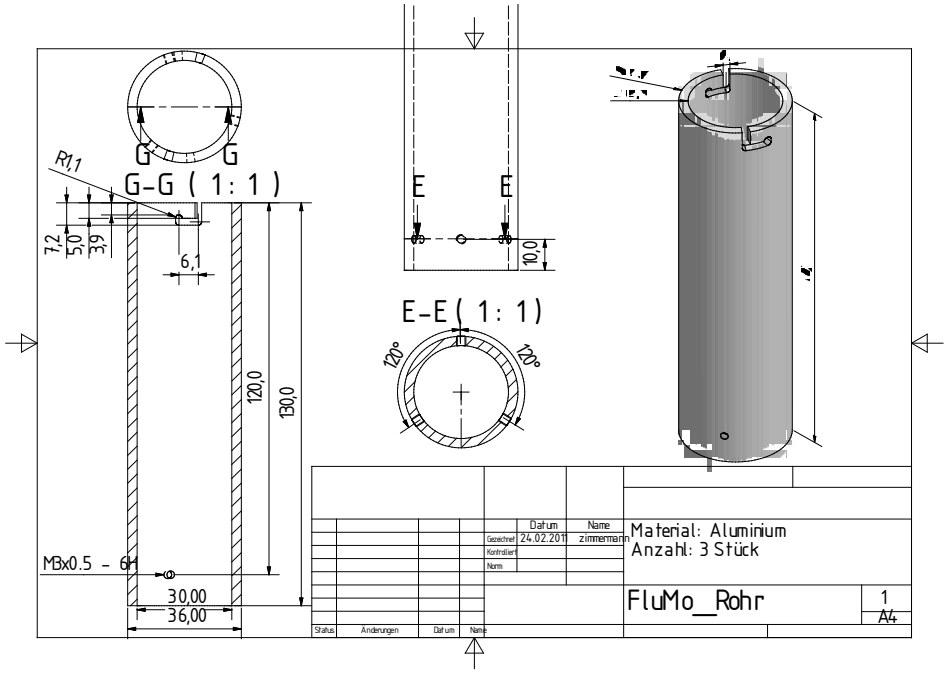

Figure A.6: Tubeof the FluMo housing

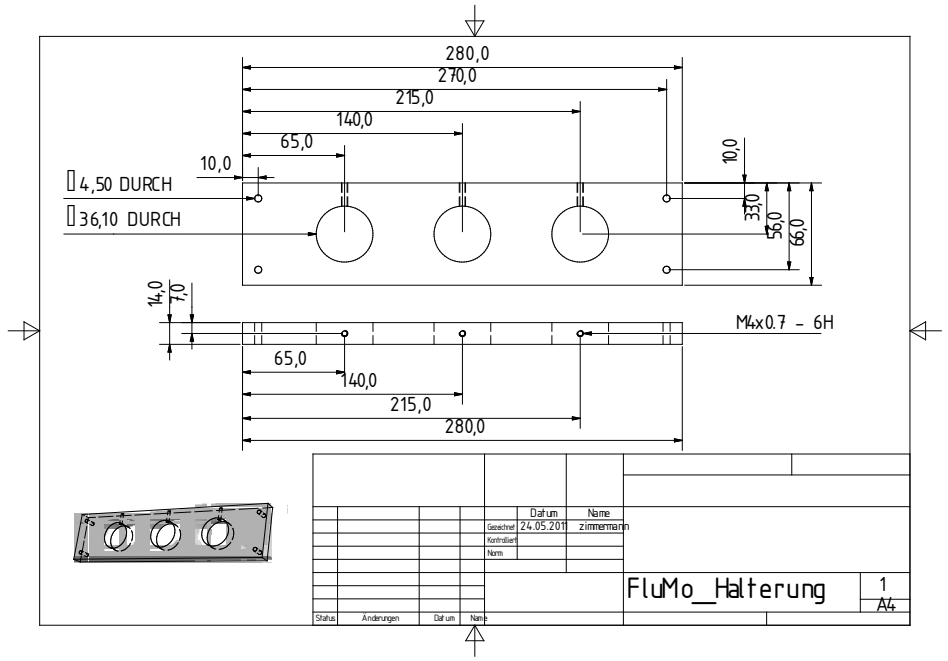

Figure A.7: Mount for the three FluMo housing tubes

A.4 Projections of the efficiency plot

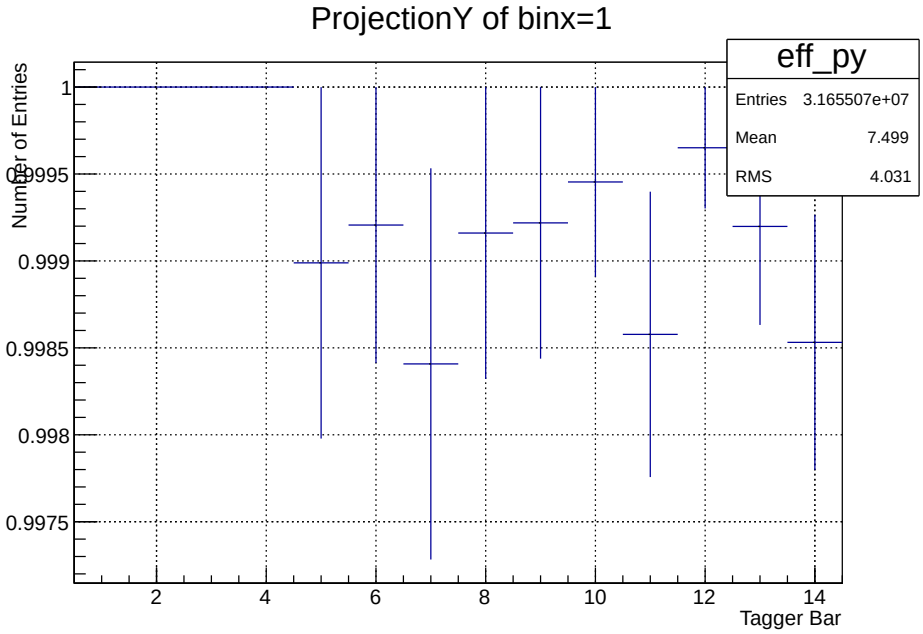

Figure A.8: Efficiency of the FluMo veto detector against the tagger bar where the corresponding electron was detected.

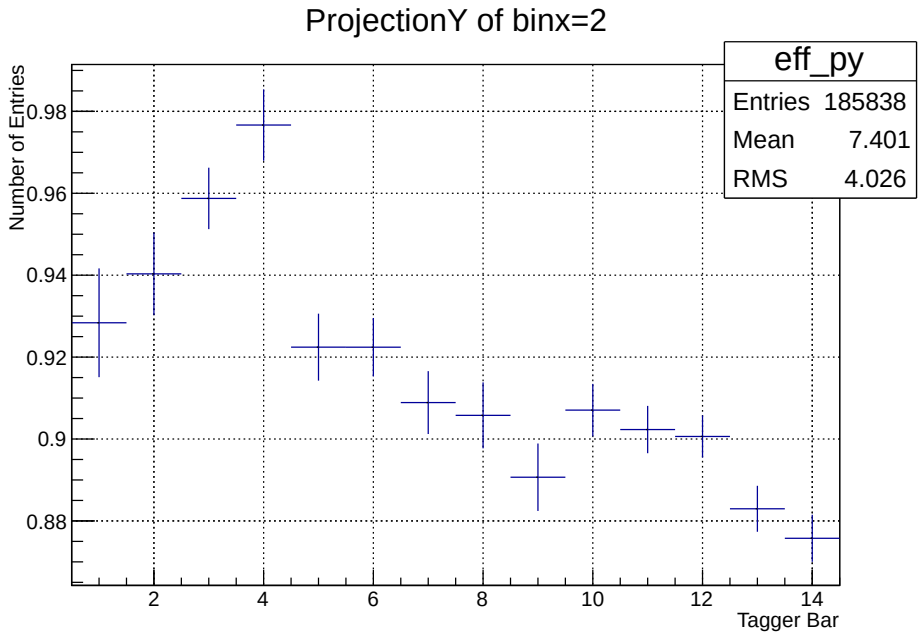

Figure A.9: Efficiency of the FluMo 1 detector against the tagger bar where the corresponding electron was detected.

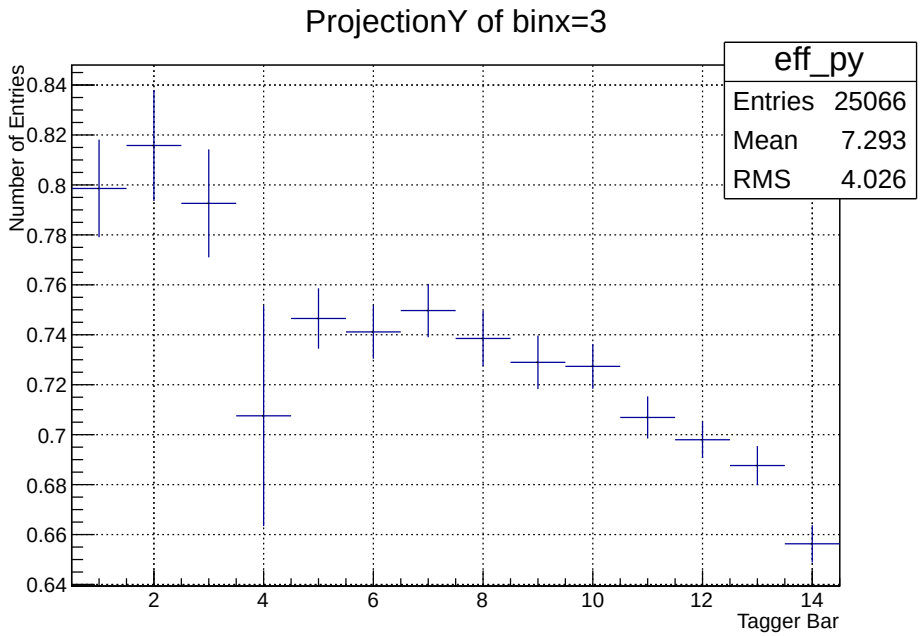

Figure A.10: Efficiency of the FluMo 2 detector against the tagger bar where the corresponding electron was detected.

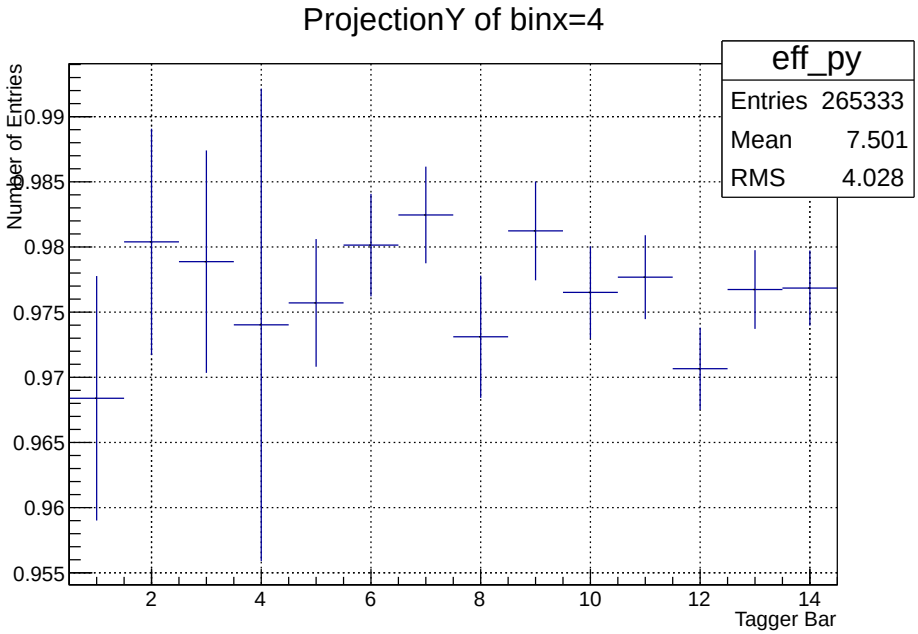

Figure A.11: Efficiency of the GIM detector against the tagger bar where the corresponding electron was detected.

Bibliography

[Ach01] Carsten Patrick Achenbach. *Aufbau eines Bleifluorid-Kalorimeter zur Messung der Paritätsverletzung in der elastischen Elektronenstreuung*. Doktorarbeit, Johannes Gutenberg Universität in Mainz, May 2001.

[Bel11] Andreas Bella. Setup of a gonimeter system for the production of linear polarized photons for the bgo-od experiment at elsa. Diplomarbeit, Rheinische Friedrich-Wilhelms-Universität Bonn, Physikalisches Institut, March 2011.

[Bie11] John Bieling. Fpga module and firmware descriptions. Internal note BGO-OD-008-2011, Rheinische Friedrich-Wilhelms-Universität Bonn, Physikalisches Institut, August 2011.

[Bol09] Boris M Bolotovskii. Vavilov – cherenkov radiation: its discovery and application. *Physics-Uspekhi*, 52(11):1099, 2009.

[Bös11] Sabine Böse. *PhD Thesis in preparation*. PhD thesis, Rheinische Friedrich-Wilhelms-Universität Bonn, Helmholtz-Institut für Strahlen- und Kernphysik, 2011.

[CB] Crystal barrel,a 4π photon spectrometer. `http://www1.cb.uni-bonn.de`.

[Cur66] Eve Curie. *Madame Curie*. S. Fischer Verlag, 1966.

[Dem09] W. Demtröder. *Experimentalphysik 4: Kern-, Teilchen- Und Astrophysik*. Experimentalphysik. Springer, 2009.

[Der11] Stephen E. Derenzo. Scintillation properties. `http://scintillator.lbl.gov`, September 2011.

[Die08] Jessica Dielmann. Entwicklung, aufbau und test eines detektors zur bestimmung des photonenflusses an der bonner photonenmarkierungsanlage. Diplomarbeit, Rheinische Friedrich-Wilhelms-Universität Bonn, Helmholtz-Institut für Strahlen- und Kernphysik, September 2008.

[EHO+04] S. Eidelman, K.G. Hayes, K.A. Olive, M. Aguilar-Benitez, C. Amsler, D. Asner, K.S. Babu, R.M. Barnett, J. Beringer, P.R. Burchat, C.D. Carone, C. Caso, G. Conforto, O. Dahl, G. D'Ambrosio, M. Doser, J.L. Feng, T. Gherghetta, L. Gibbons, M. Goodman, C. Grab, D.E. Groom, A. Gurtu, K. Hagiwara, J.J. Hernández-Rey, K. Hikasa, K. Honscheid, H. Jawahery, C. Kolda, Kwon Y., M.L. Mangano, A.V. Manohar, J. March-Russell, A. Masoni, R. Miquel, K. Mönig, H. Murayama, K. Nakamura, S. Navas, L. Pape, C. Patrignani, A. Piepke, G. Raffelt, M. Roos, M. Tanabashi, J. Terning, N.A. Törnqvist, T.G. Trippe, P. Vogel, C.G. Wohl, R.L. Workman, W.-M. Yao, P.A. Zyla, B. Armstrong, P.S. Gee, G. Harper, K.S. Lugovsky, S.B. Lugovsky, V.S. Lugovsky, A. Rom, M. Artuso, E. Barberio, M. Battaglia, H. Bichsel, O. Biebel, P. Bloch, R.N. Cahn, D. Casper, A. Cattai, R.S. Chivukula, G. Cowan, T. Damour, K. Desler, M.A. Dobbs, M. Drees, A. Edwards, D.A.

Edwards, V.D. Elvira, J. Erler, V.V. Ezhela, W. Fetscher, B.D. Fields, B. Foster, D. Froidevaux, M. Fukugita, T.K. Gaisser, L. Garren, H.-J. Gerber, G. Gerbier, F.J. Gilman, H.E. Haber, C. Hagmann, J. Hewett, I. Hinchliffe, C.J. Hogan, G. Höhler, P. Igo-Kemenes, J.D. Jackson, K.F. Johnson, D. Karlen, B. Kayser, D. Kirkby, S.R. Klein, K. Kleinknecht, I.G. Knowles, P. Kreitz, Yu.V. Kuyanov, O. Lahav, P. Langacker, A. Liddle, L. Littenberg, D.M. Manley, A.D. Martin, M. Narain, P. Nason, Y. Nir, J.A. Peacock, H.R. Quinn, S. Raby, B.N. Ratcliff, E.A. Razuvaev, B. Renk, G. Rolandi, M.T. Ronan, L.J. Rosenberg, C.T. Sachrajda, Y. Sakai, A.I. Sanda, S. Sarkar, M. Schmitt, O. Schneider, D. Scott, W.G. Seligman, M.H. Shaevitz, T. Sjöstrand, G.F. Smoot, S. Spanier, H. Spieler, N.J.C. Spooner, M. Srednicki, A. Stahl, T. Stanev, M. Suzuki, N.P. Tkachenko, G.H. Trilling, G. Valencia, K. van Bibber, M.G. Vincter, D. Ward, B.R. Webber, M. Whalley, L. Wolfenstein, J. Womersley, C.L. Woody, O.V. Zenin, and R.-Y. Zhu. Review of Particle Physics. *Physics Letters B*, 592:1+, 2004.

[ELS05] Das konzept von elsa. `http://www-elsa.physik.uni-bonn.de/Beschleuniger/elsa.html`, January 2005.

[ET] ET Enterprises. *9111B series datasheet*.

[Fer] Fermilab. Lecroy 821 quad discriminator. `http://www-esd.fnal.gov/esd/catalog/main/lcrynim/821-spec.htm`.

[FT37] I. M. Frank and I. E. Tamm. "coherent visible radiation of fast electrons passing through matter". *Dokl. Akad. Nauk. USSR*, 14:109 – 114, 1937.

[Goe11] Johannes Goetze. Building a base for the bgo-od gim. BCGS Internship presentation, April 2011.

[Ham] Hamamatsu. *Photomultiplier Tubes*.

[Ham08] Daniel Hammann. Test und betrieb der prototyp-driftkammer für das b1-spektrometer. Diplomarbeit, Rheinische Friedrich-Wilhelms-Universität Bonn, Physikalisches Institut, November 2008.

[icv37] P. A. Čerenkov. Visible radiation produced by electrons moving in a medium with velocities exceeding that of light. *Phys. Rev.*, 52(4):378–379, Aug 1937.

[Kon01] Michael Konrad. Ortssensitiver detektor für hochenergetische photonen bei höchsten raten. Diplomarbeit, Rheinische Friedrich-Wilhelms-Universität Bonn, Helmholtz-Institut für Strahlen- und Kernphysik, March 2001.

[Leo94] W.R. Leo. *Techniques for nuclear and particle physics experiments: a how-to approach*. Springer, 1994.

[Loh90] E Lohrmann. *Einführung in die Elementarteilchenphysik*. Teubner Studienbücher. Teubner, 1990.

[McG08] William R McGehee. The gamma intensity monitor at the crystal-barrel-experiment. Bachelor's thesis, Massachusetts Institute of Technology. Dept. of Physics., June 2008.

[Mes11] Francesco Messi. The afa board (an active splitter for analog signals). Internal note BGO-OD-009-2011, Rheinische Friedrich-Wilhelms-Universität Bonn, Physikalisches Institut, September 2011.

[MOM09] Momo. `http://b1.physik.uni-bonn.de/ExperimentalSetup/Momo`, July 2009.

[NG10] K Nakamura and Particle Data Group. Review of particle physics. *Journal of Physics G: Nuclear and Particle Physics*, 37(7A):075021, 2010.

[Ram07] Alexander Ramseger. Vorbereitung und test des flugzeitdetektors für das crystal-barrel-experiment an elsa. Diplomarbeit, Rheinische Friedrich-Wilhelms-Universität Bonn, Physikalisches Institut, Februar 2007.

[Sai] Saint-Gobain Crystals. *BC-400,BC-404,BC-408,BC-412,BC-416 Premium Plastic Scintillators*.

[Sch10] Timothy Schwan. Test und inbetriebnahme der driftkammern für das bgo-od-spektrometer. Diplomarbeit, Rheinische Friedrich-Wilhelms-Universität Bonn, Physikalisches Institut, April 2010.

[Sie10] Georg Siebke. Design of the bgo-od tagging system and test of a detector prototype. Diplomarbeit, Rheinische Friedrich-Wilhelms-Universität Bonn, Physikalisches Institut, November 2010.

[YYO+96] Y. Yoshizawa, H. Yamaguchi, N. Ooishi, H. Suzuki, and S. Suzuki. The study of countrate stability of photomultiplier tube with different types of voltage dividers. *Nuclear Science, IEEE Transactions on*, 43(3):1656 –1660, jun 1996.

[Zre70] V. P. Zrelov. *Cherenkov radiation in high-energy physikcs*, volume Part 1, Cherenkov Radiation in Isotropic and Anisotropic Media: Theory and Experimental Verification. Israel Program for Scientific Translations, 1970.

List of Figures

List of Tables